Future Astrophysical Targets for Intensity Interferometry

Neal Dalal, Marios Galanis, Charles Gammie, Samuel Gralla, Norman Murray




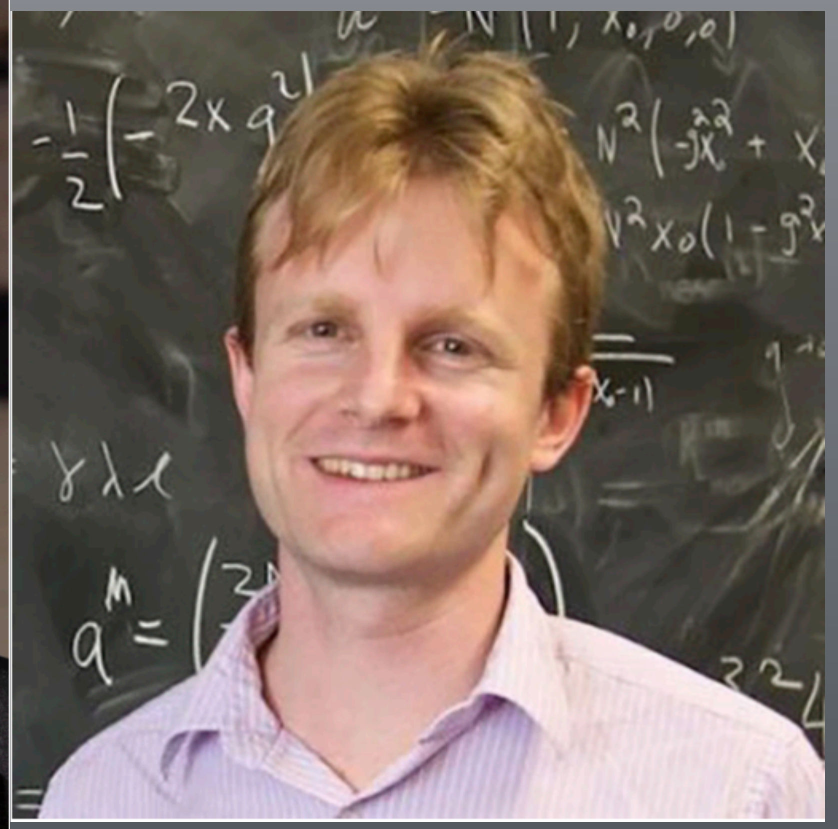

Intensity Interferometry

Hanbury Brown & Twiss

- Similar to interferometry in the radio or millimeter band (amplitude interferometry)
- Use large base lines **B** and short wavelengths λ to get high angular resolution
  - $\theta \sim \lambda/B$
  - $\lambda \sim 5000$ angstroms or 5×10^{-5} cm, $B \sim 10^4$ km, $\theta \sim 0.01\mu$ arcseconds
  - AGN disks $R_s \sim 3x10^8$ km, $D \sim 100$Mpc, $\theta \sim 20\mu$ arcseconds
  - Stellar disks $R_\odot \sim 7x10^{10}$ cm, $D \sim 10$ pc, $\theta \sim 0.5$ milliarcseconds
    - Can get many resolution elements across the stellar disk

Intensity Interferometry

Hanbury Brown & Twiss

- Use two or more telescopes separated by **B**
  - $\mathbf{B} = \mathbf{B}_{\perp} + (\mathbf{B} \cdot \mathbf{n})\, \mathbf{n}$ $\quad \mathbf{B}_{\perp}/\lambda \equiv (u,v)$
- Record the arrival times of photons (intensity $I(t)=|E(t)|^2$) at each telescope
- At some later time, correlate the signals

1. One frequency $E=a\, e^{i\omega t}$

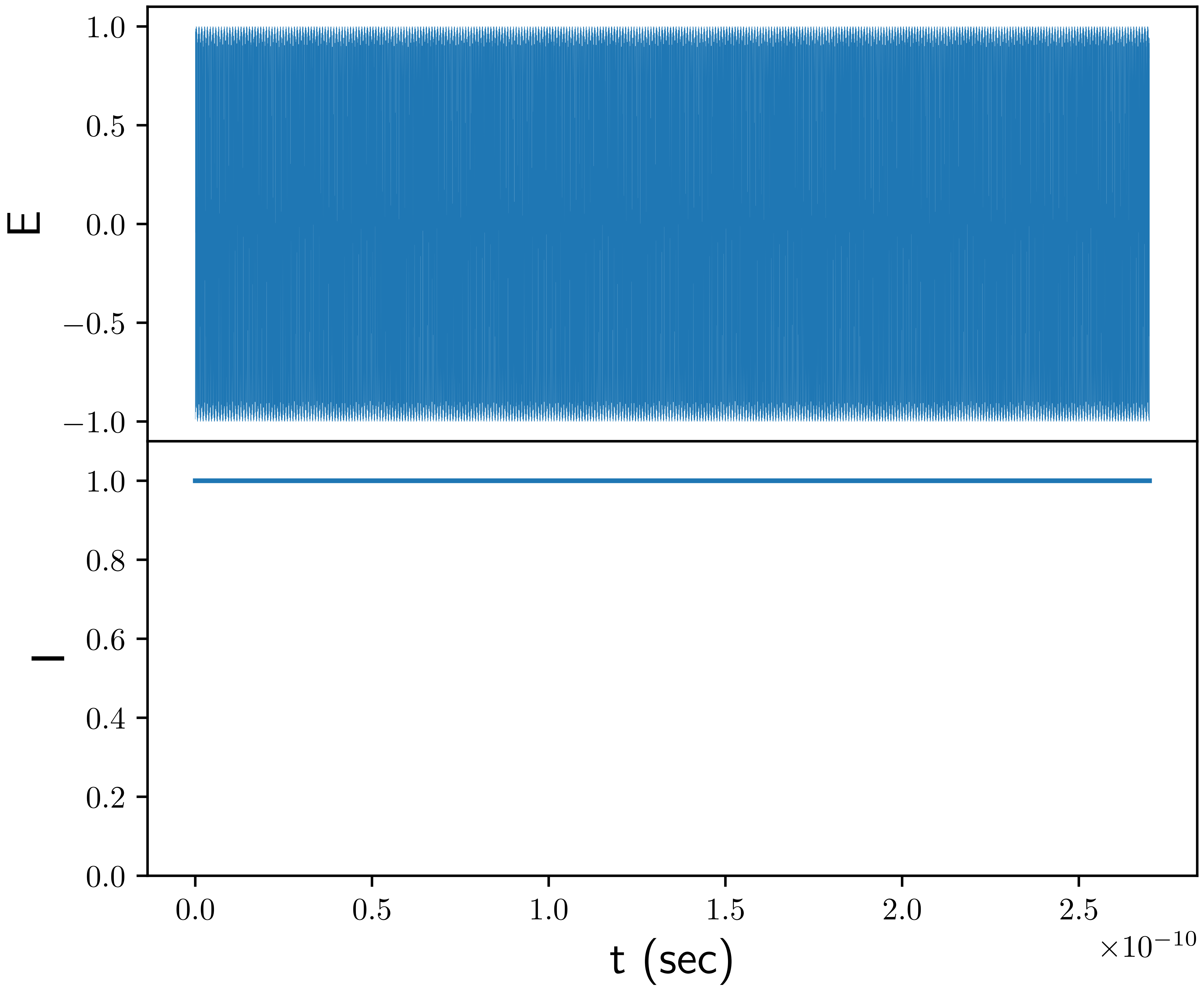

Intensity Interferometry

Hanbury Brown & Twiss

- Use two or more telescopes separated by **B**
  - $\mathbf{B} = \mathbf{B}_\perp + (\mathbf{B} \cdot \mathbf{n})\, \mathbf{n}$ $\mathbf{B}_\perp/\lambda \equiv (u,v)$
- Record the arrival times of photons (intensity $I(t)=|E(t)|^2$) at each telescope
- At some later time, correlate the signals

1. One frequency $E=a\, e^{i\omega t}$
2. Two frequencies $E = a_1\, e^{i\omega_1 t} + a_2\, e^{i\omega_2 t}$

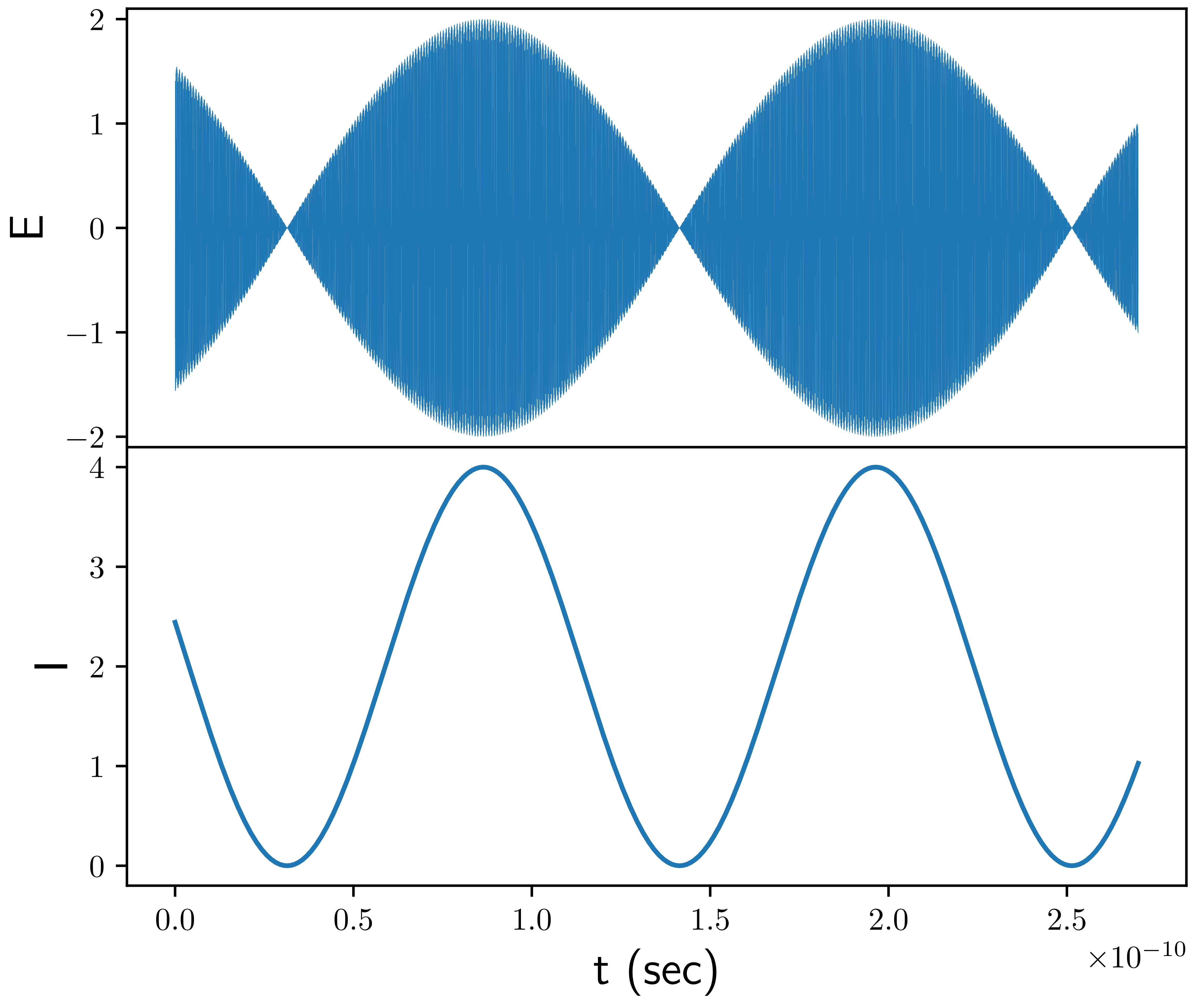

Intensity Interferometry

Hanbury Brown & Twiss

- Use two or more telescopes separated by **B**
  - $\mathbf{B} = \mathbf{B}_\perp + (\mathbf{B} \cdot \mathbf{n})\,\mathbf{n}$ $\quad \mathbf{B}_\perp/\lambda \equiv (u,v)$
- Record the arrival times of photons (intensity $I(t)=|E(t)|^2$) at each telescope
- At some later time, correlate the signals

1. One frequency $E=a\,e^{i\omega t}$
2. Two frequencies $E = a_1\,e^{i\omega_1 t} + a_2\,e^{i\omega_2 t}$
3. Sum of many frequencies

$$E = \Sigma_j\, a_j\, e^{i\omega_j t}$$

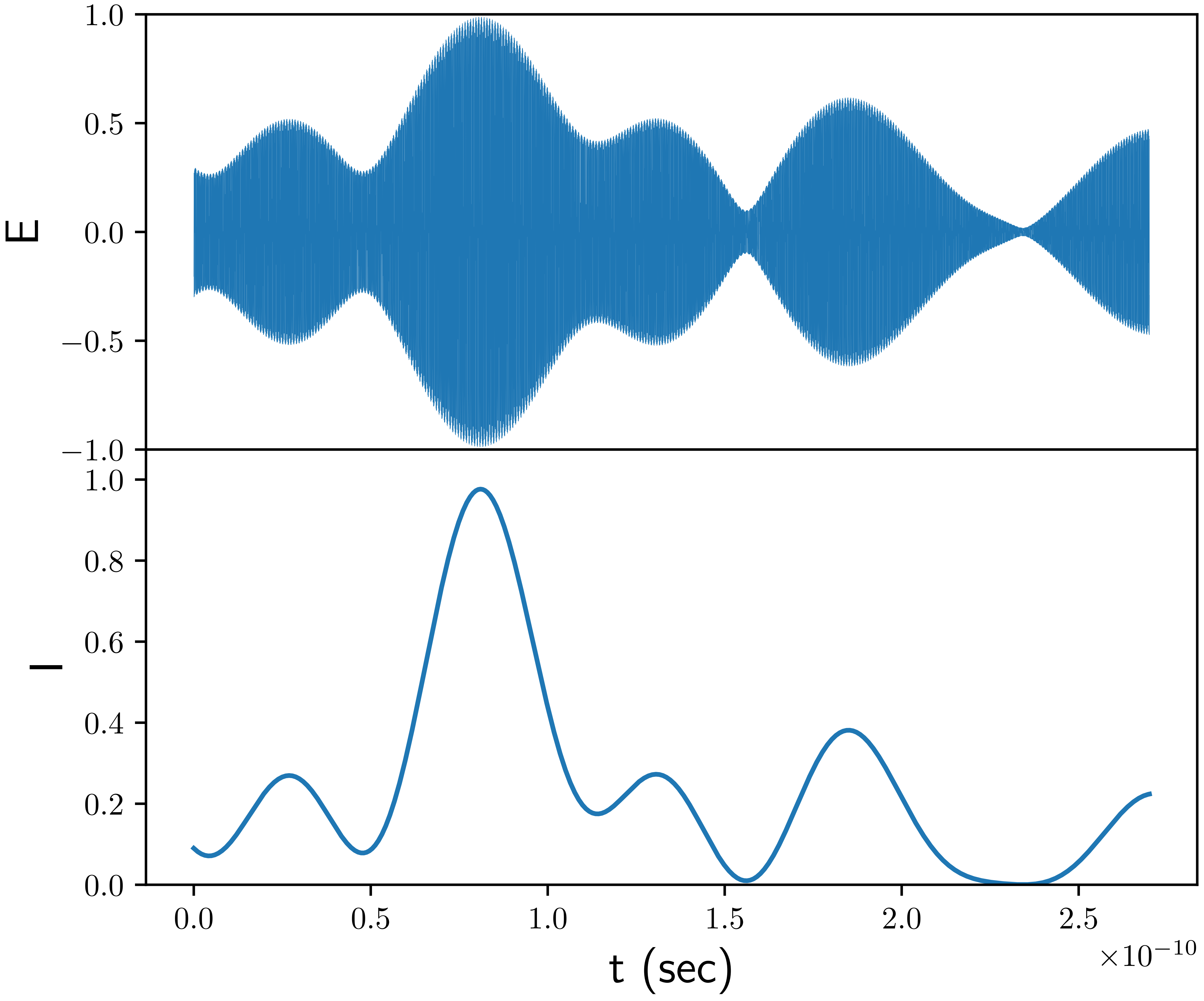

Intensity Interferometry

Hanbury Brown & Twiss

- The count rate of photons can vary by order unity
- Nearby AGN will have count rates of 10^6 photons per second

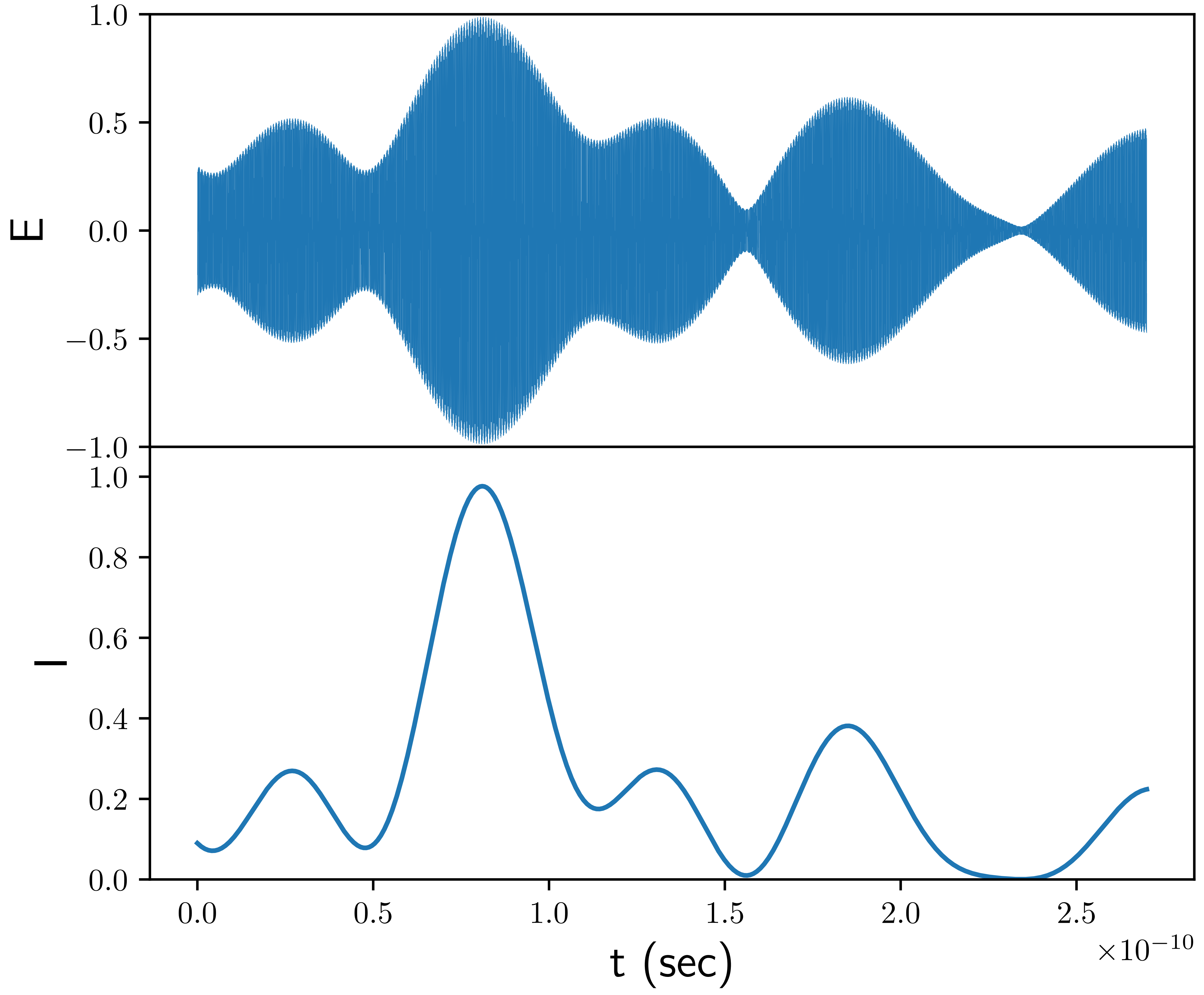

1. This is not shot noise!

Intensity Interferometry

Hanbury Brown & Twiss (1956)

Hanbury Brown and Twiss measured the correlation at different separations d, ranging from 2.5 to 9.2 meters, to find the angular size of Sirius, 0.0063"

Note that the correlation of an extended source falls off more rapidly than that of a point source

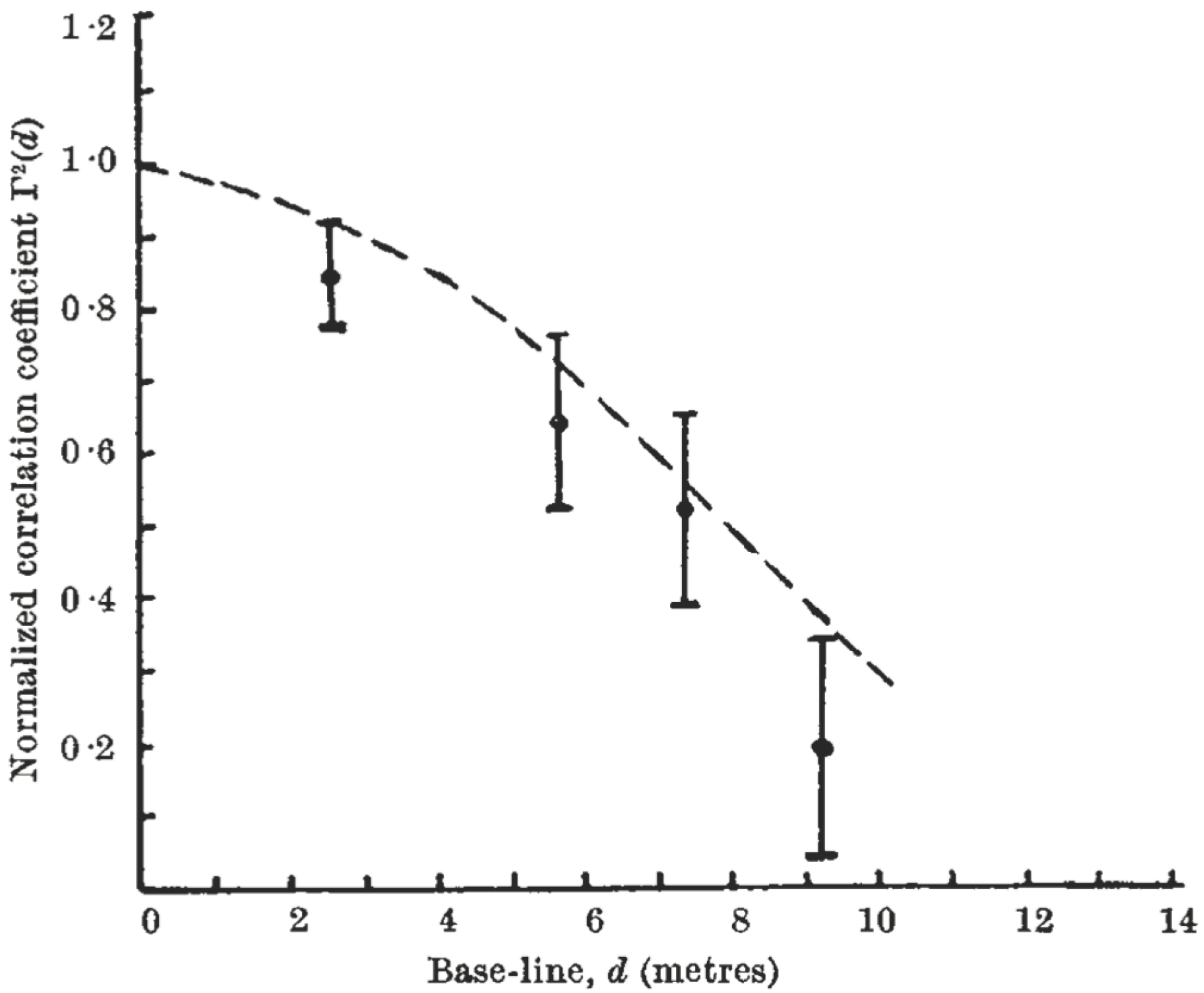

Fig. 2. Comparison between the values of the normalized correlation coefficient $\Gamma^2(d)$ observed from Sirius and the theoretical values for a star of angular diameter 0·0063". The errors shown are the probable errors of the observations

Base-line d = $|\mathbf{B}_{\perp}/\lambda| = |(u,v)|$

Photon correlations

To maximize SNR, we want lots of photons and precise timing.

Slide credit: Neal Dalal

SPADs

Single Photon Avalance Diodes

HAMAMATSU
PHOTON IS OUR BUSINESS

Products Applications Why Hamamatsu? Resources Support Our company Investors CAN

Home > Products > Optical sensors >

MPPCs (SiPMs) / SPADs

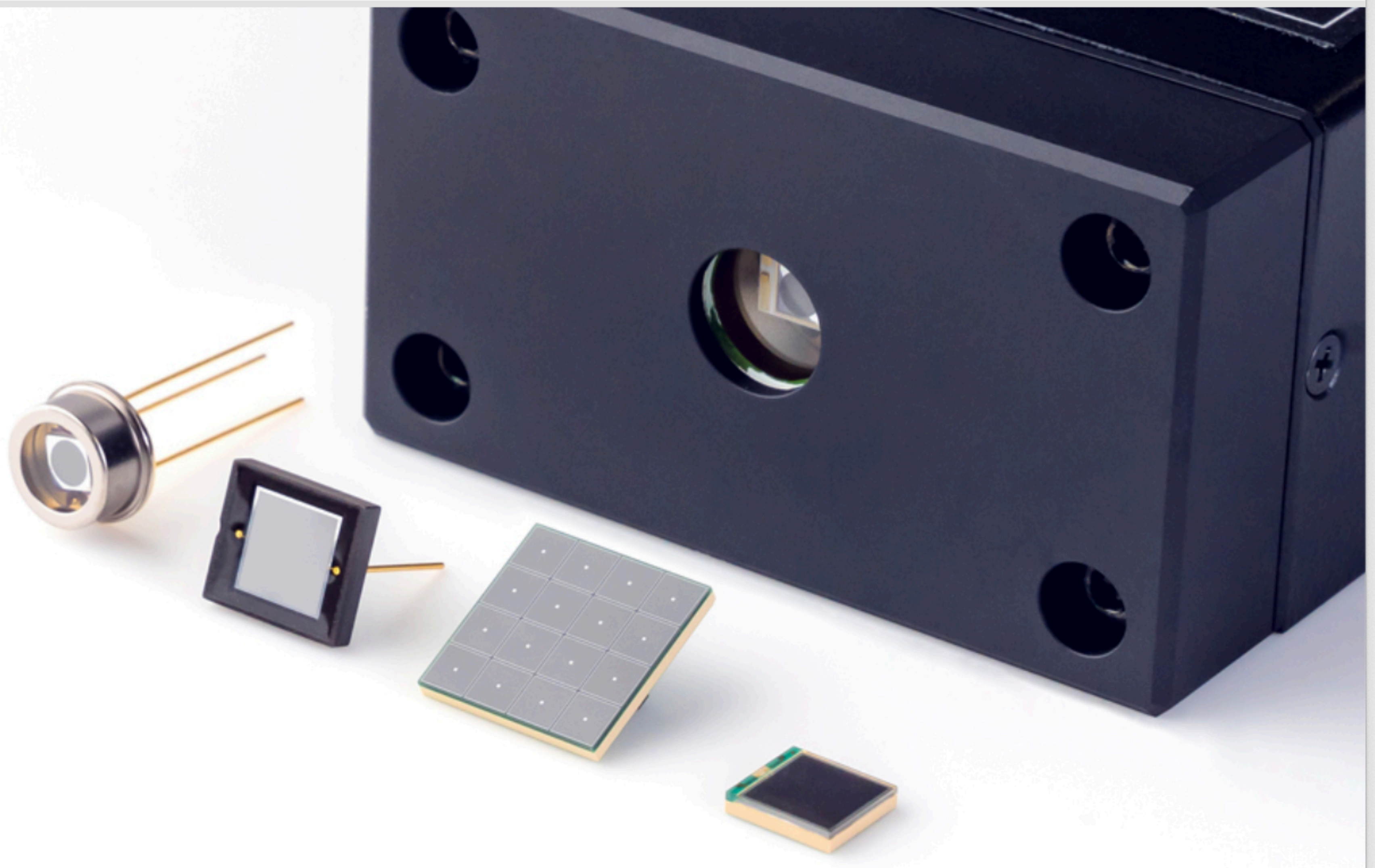

MPPC (Multi-Pixel Photon Counter) is a device called SiPM, which is a photon counting device that is a multi-pixelized Geiger mode APD. While it is an optical semiconductor device, it has an excellent detection ability, so this device can be used in a variety of applications to detect very low-level light at the photon counting level.
Hamamatsu's SPAD (Single Photon Avalanche Diode) is an element with a structure of a single pixel that combines a Geiger mode APD and a quenching resistor into one set. It is an optical semiconductor element that enables photon counting.

SPADs

Single Photon Avalance Diodes

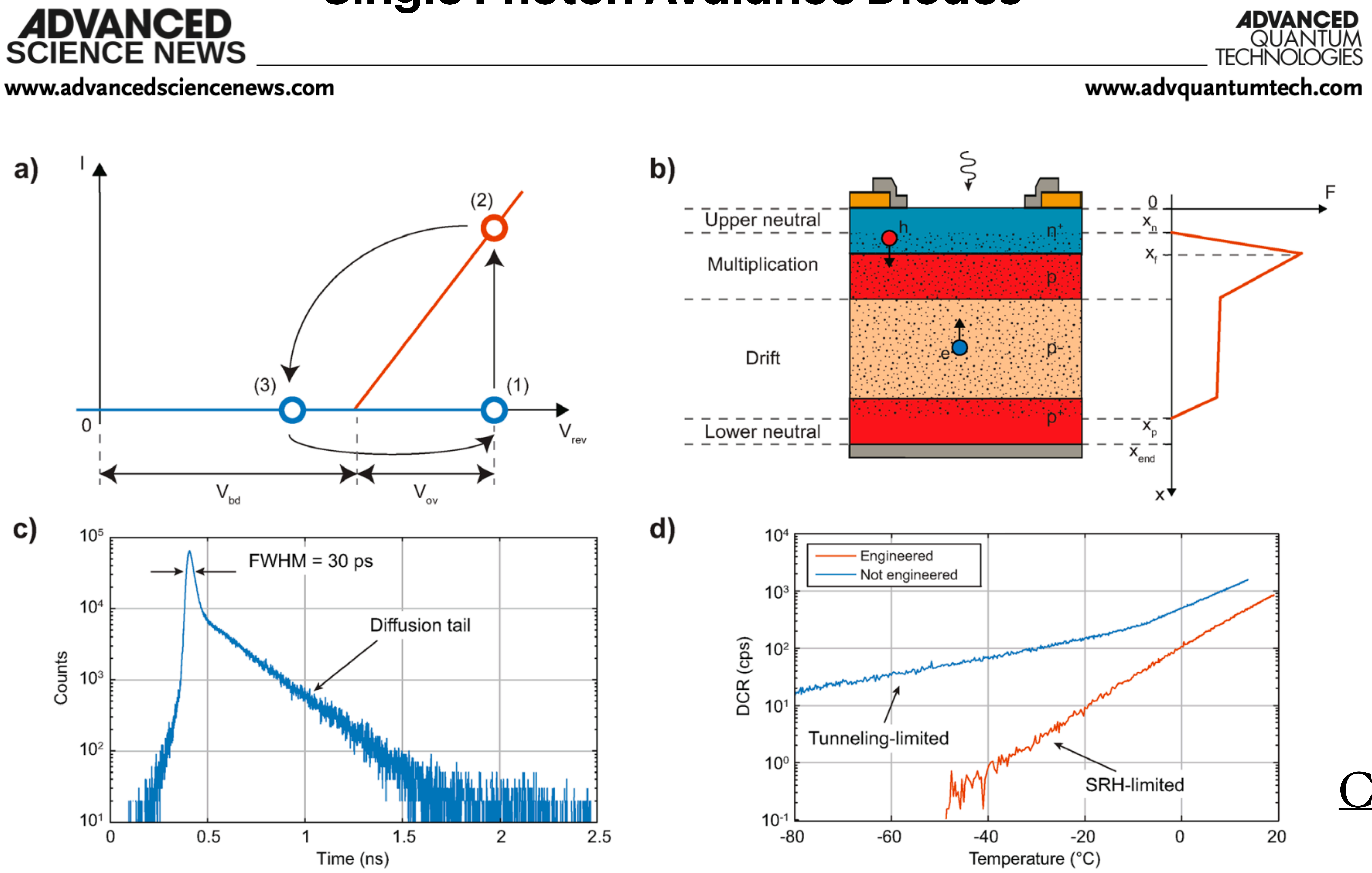

Ceccarelli+ (2021)

SNSPDs

Superconducting Nanowire Single Photon Detector

Rev. Sci. Instrum. **82**, 071101 (2011)

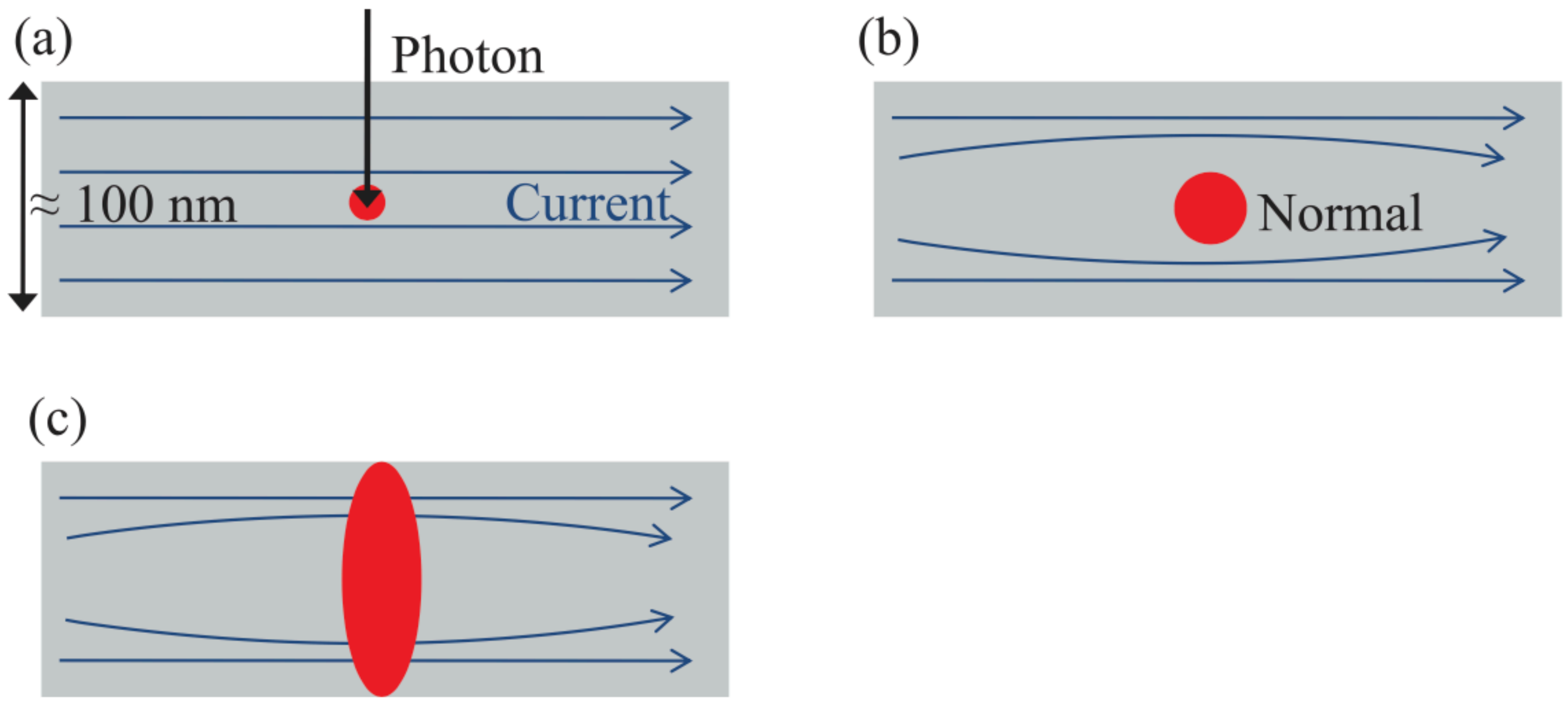

FIG. 8. (Color online) A section of a superconducting nanowire single-photon detector is shown with a bias current just below the critical current density that would drive the wire normal. (a) An incoming photon creates a small normal region within the nanowire. (b) The superconducting current is expelled from the normal region, increasing the current density in the adjacent areas of the nanowire. (c) That increase in current density is enough to drive those adjacent regions normal, which in turn results in a measurable voltage drop across the detector.

Eisaman+ 2024

SNSPDs

Oripov+ 2023

Superconducting Nanowire Single Photon Detector Array

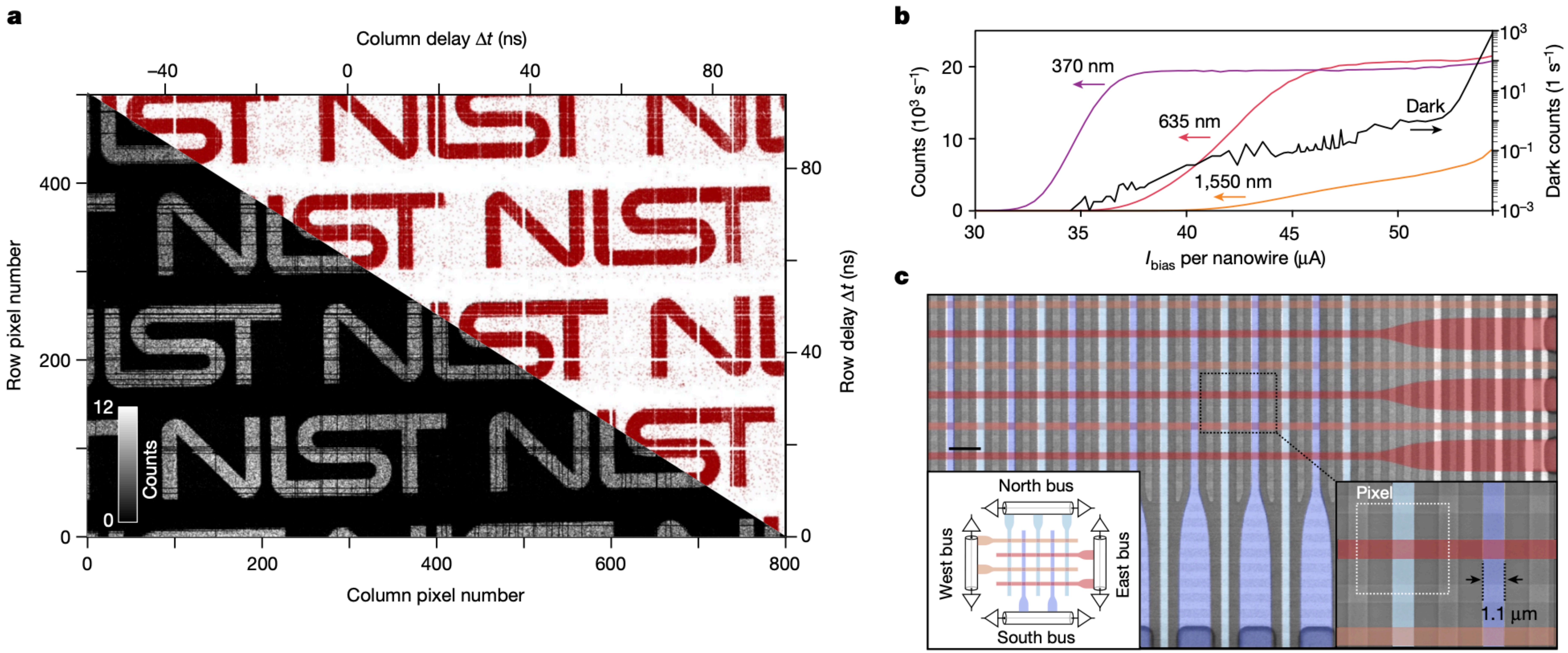

Fig. 1 | Overview of the 800 × 500 camera. a, Imaging at 370 nm, with raw time-delay data from the buses shown as individual dots in red and binned 2D histogram data shown in black and white. **b**, Count rate as a function of bias current for various wavelengths of light as well as dark counts. **c**, False-colour scanning electron micrograph of the lower-right corner of the array, highlighting the interleaved row and column detectors. Lower-left inset, schematic diagram showing detector-to-bus connectivity. Lower-right inset, close-up showing 1.1-μm detector width and effective 5 × 5-μm pixel size. Scale bar, 5 μm.

SNSPDs

Oripov+ 2023

Superconducting Nanowire Single Photon Detector Array

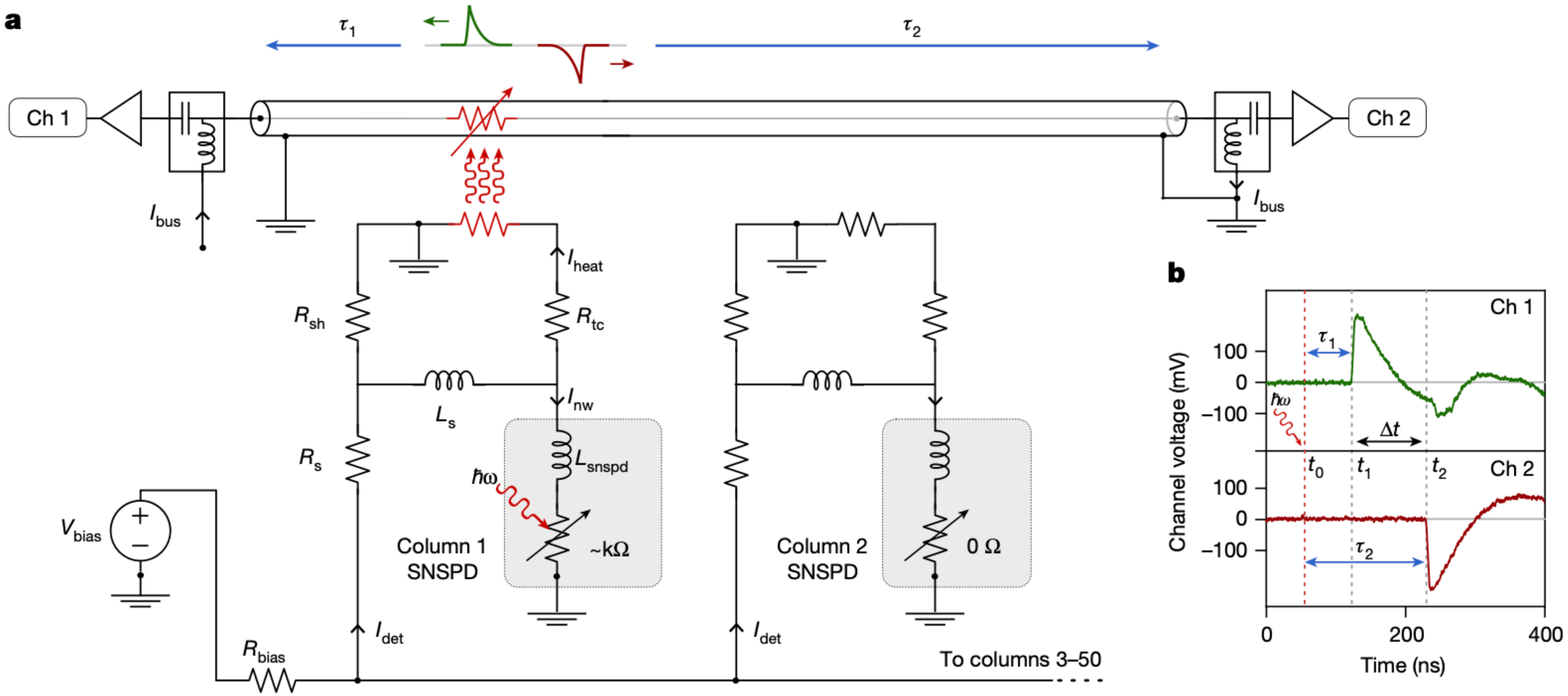

Fig. 2 | Electrical operation of the detectors and readout bus. a, Circuit diagram of a bus and one section of 50 detectors with ancillary readout components. SNSPDs are shown in the grey boxes and all other components are placed outside the imaging area. A photon that arrives at time t_0 has its location determined by a time-of-flight readout process based on the time-of-arrival difference $t_2 - t_1$. **b**, Oscilloscope traces from a photon detection showing the arrival of positive (green) and negative (red) pulses at times t_1 and t_2, respectively.

Possible Astrophysical Targets

- AGN
- Resolved Asteroseismology
- Photon rings
- Tidal Disruption Events
- Supernovae

Possible Astrophysical Targets

- AGN
  - Disk angular size
    - Measure H_0
  - Disk scale height
    - Thin versus thick
  - Map Broad Line Region
    - Determine where outflows emerge
- Resolved Asteroseismology
  - 2D power spectra (velocity versus l)
    - Run of Temperature
    - Rotational splitting $\Rightarrow$ Internal differential rotation

Geometric measurement of H_0

AGN Broad Line Region

Credit: Neal Dalal

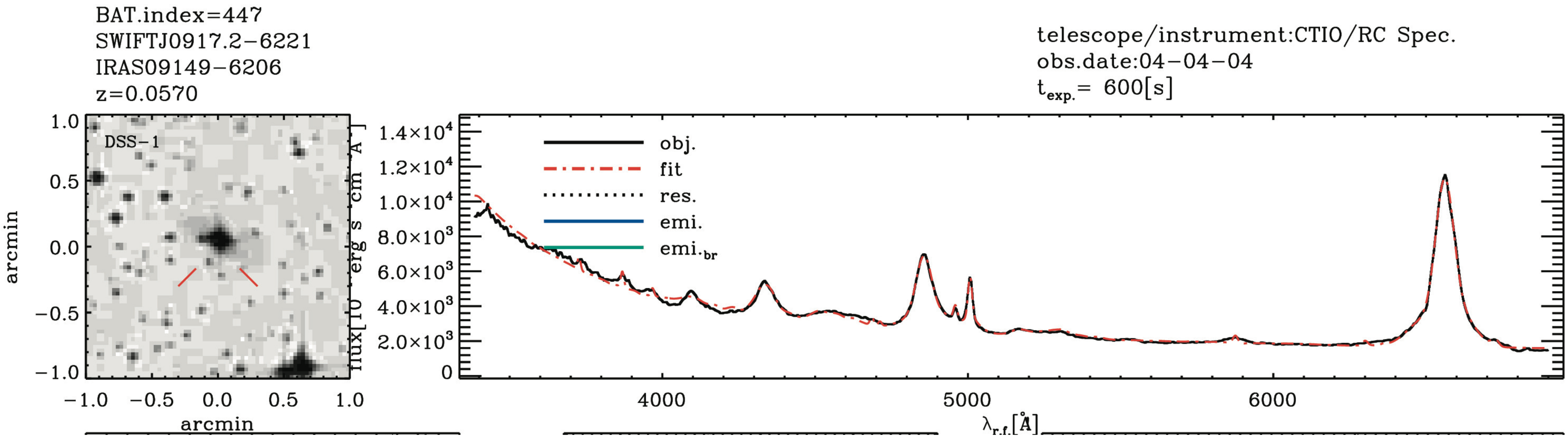

Credit: Neal Dalal

AGN variability

- AGN luminosity varies over time, for both continuum and lines.
- But line variability **lags** the continuum variability.
- Time lags can be days - months

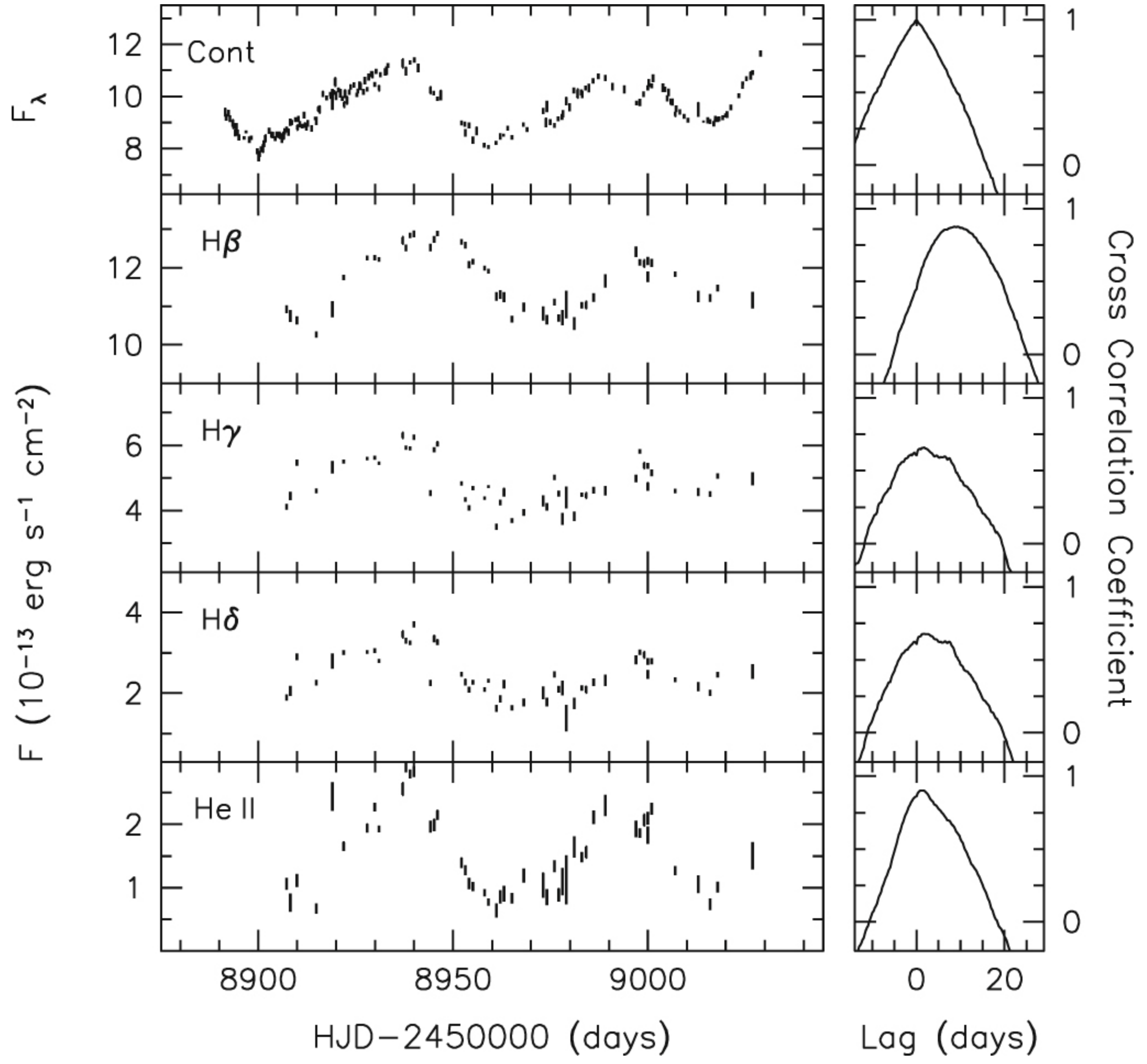

Bentz et al. (2021)

Credit: Neal Dalal

Measuring H_0

- Time lags between line variability & continuum variability tell us physical size of line-emitting region.
- Interferometry tells us the angular size of the same line-emitting region (same photons)
- Comparing the two tells us the angular diameter distance to the AGN
- Since these are line emitters, we also have redshift
- Distance + redshift = H_0

Credit: Neal Dalal

IRAS 09149-6206

24hours, CTA-sized array

For AGN science, all these numbers are interesting!

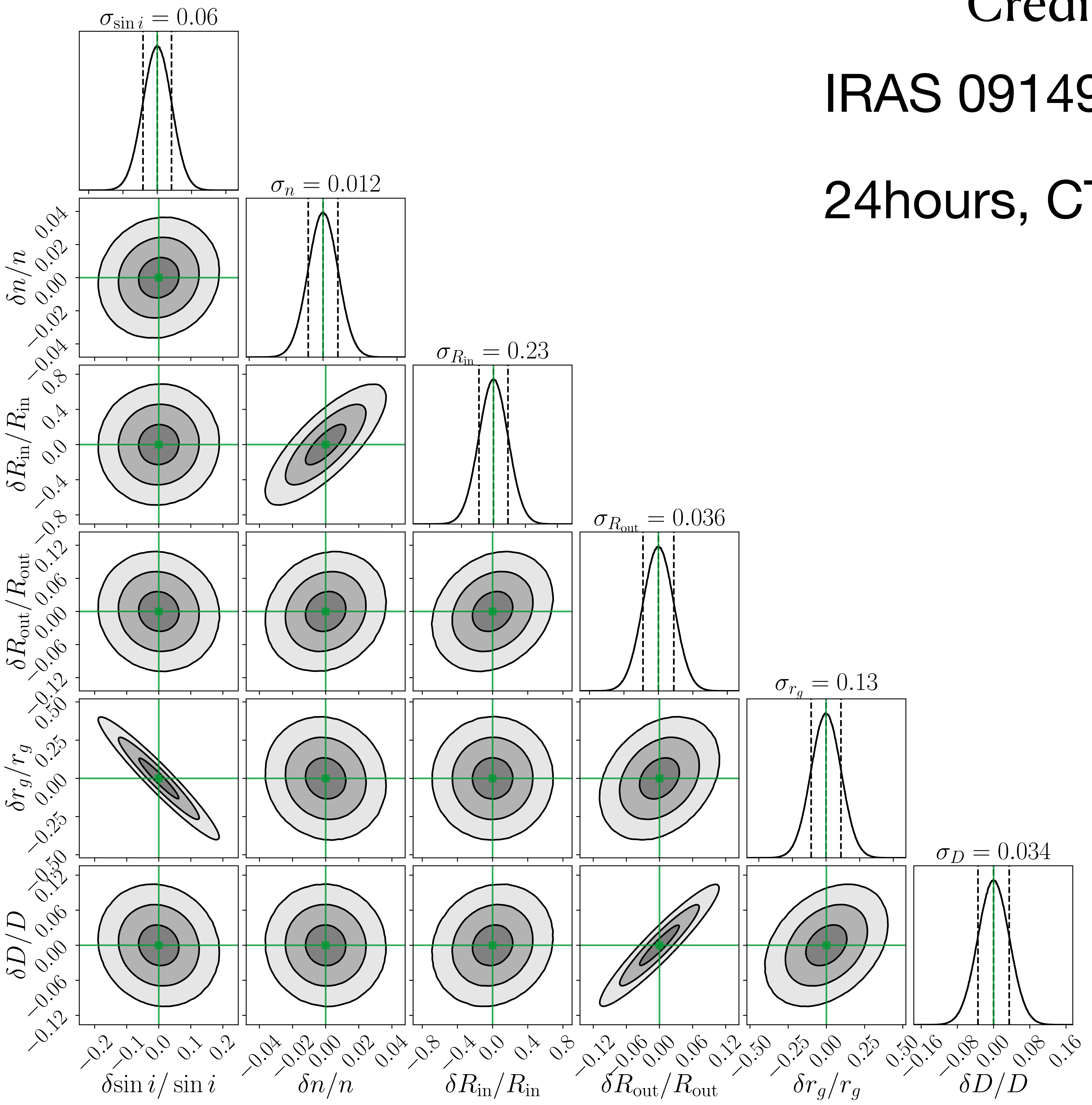

Distance is interesting for cosmology

AGN: Thin Disks?

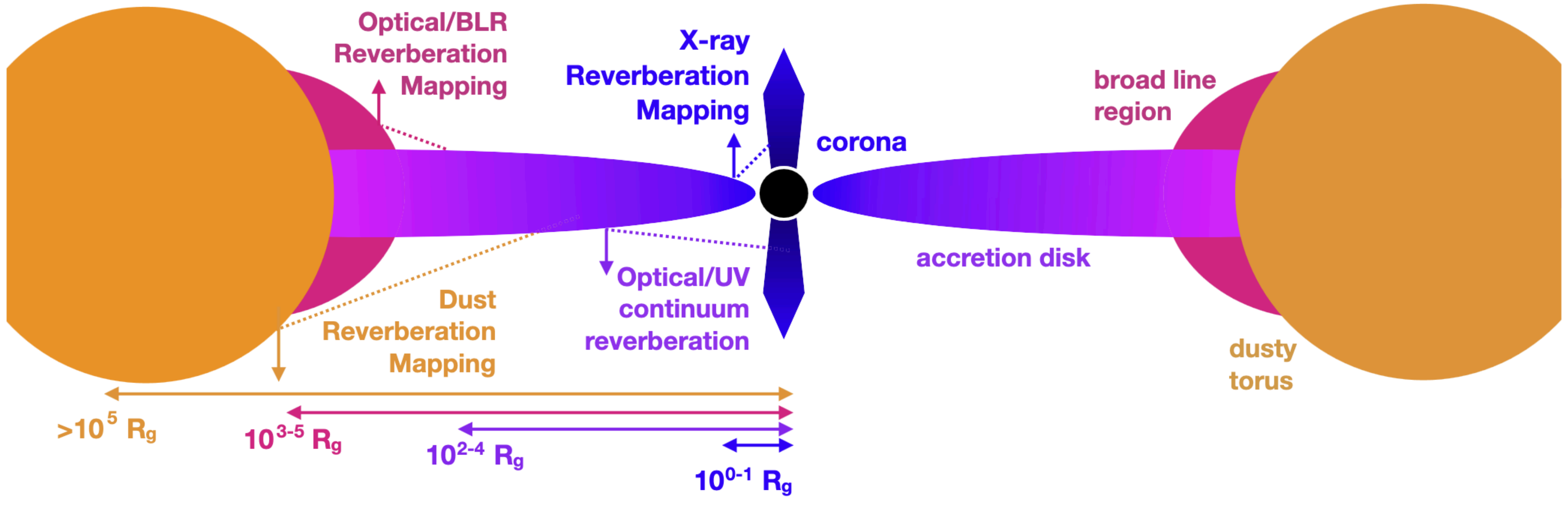

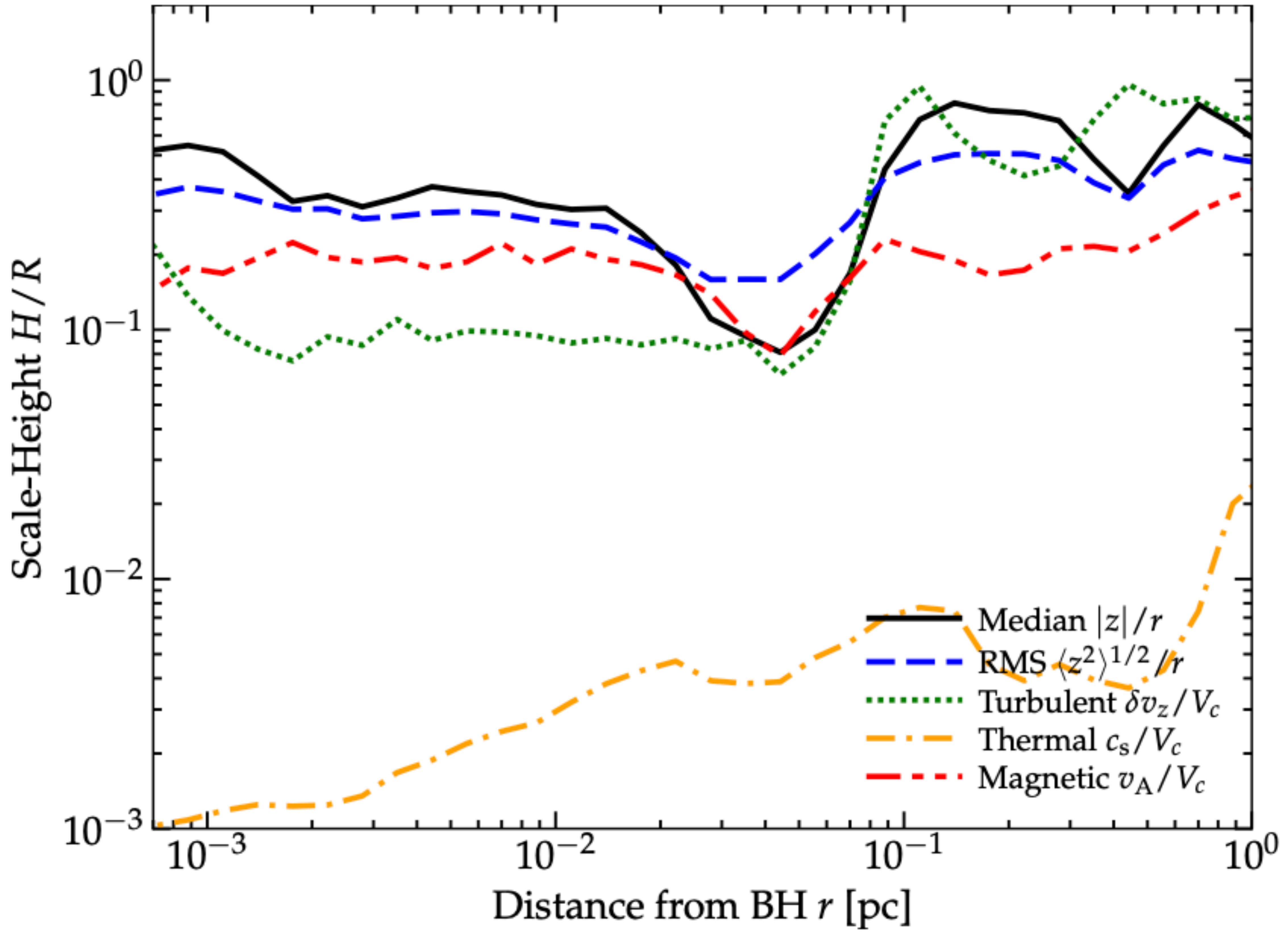

AGN: Thin Disks?

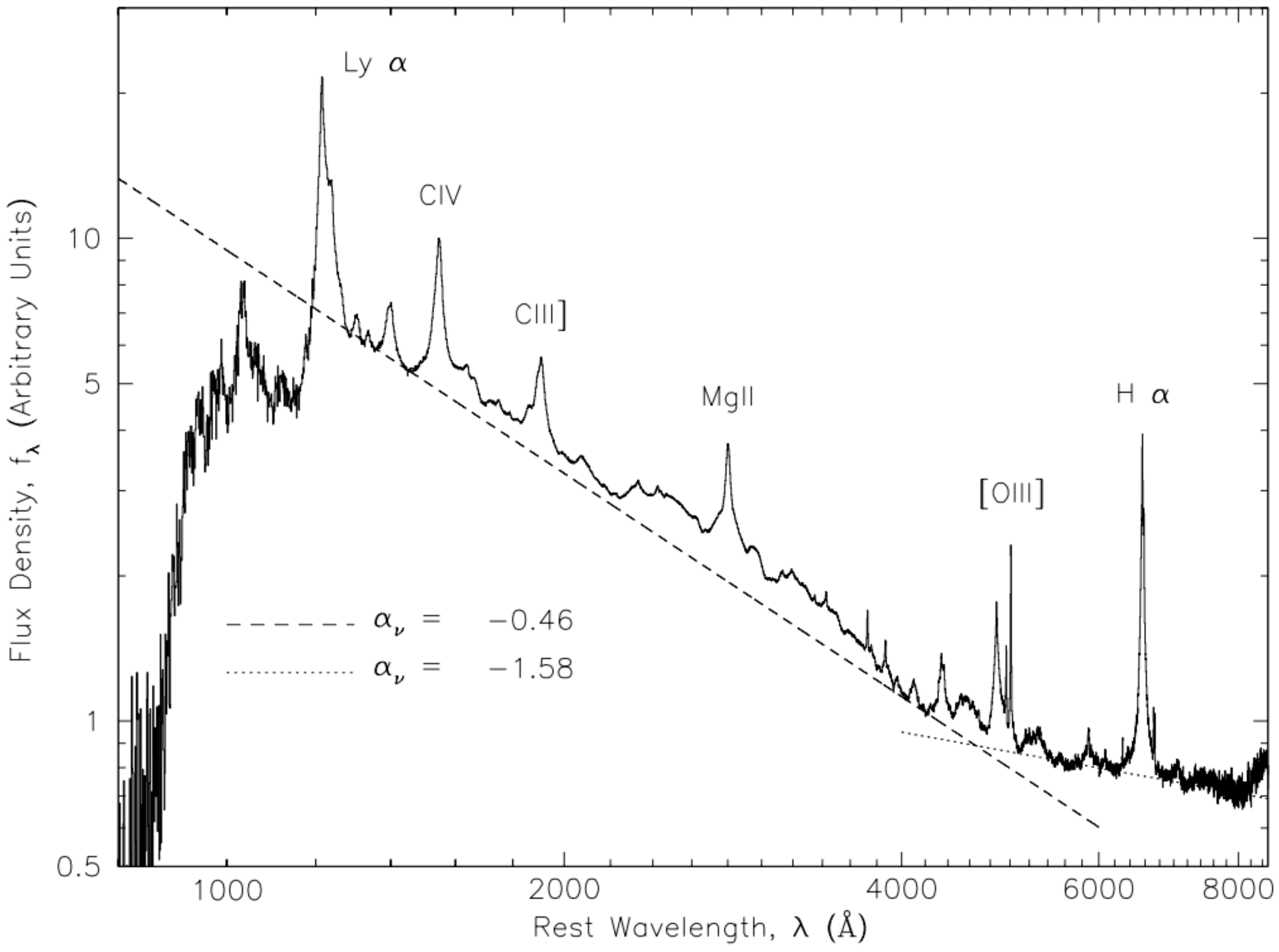

FIG. 3.—Composite quasar spectrum using median combining. Power-law fits to the estimated continuum flux are shown. The resolution of the input spectra is ≈1800, which gives a wavelength resolution of about 1 Å in the rest frame.

Ferrarese & Merritt 2000

BAL Outflows & Galaxy Evolution

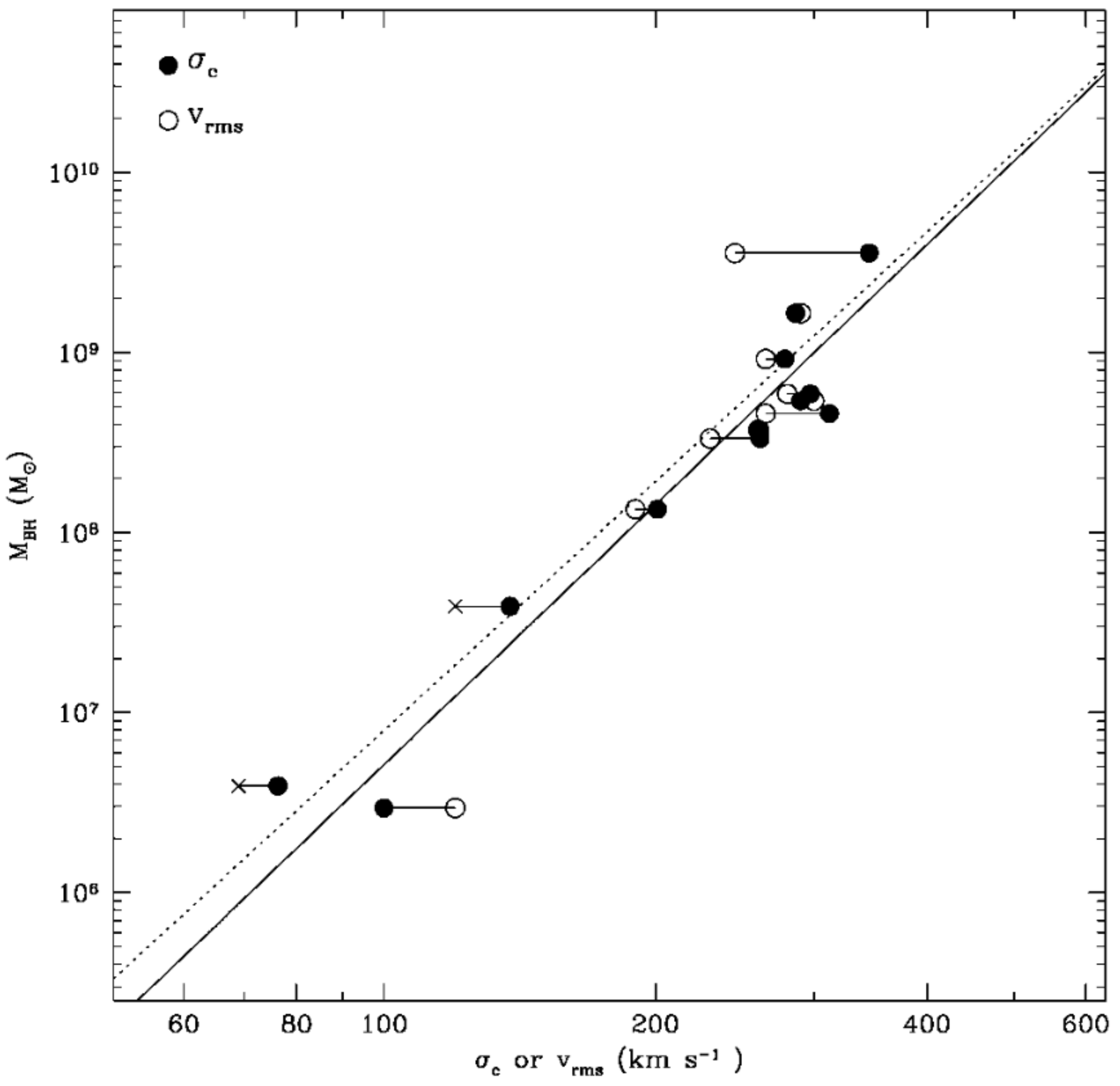

FIG. 2.—BH mass vs. the central velocity dispersion σ_c of the host elliptical galaxy or bulge (*filled circles*) or the rms velocity v_{rms} measured at one-fourth of the effective radius (*open circles*). Crosses represent lower limits in v_{rms}. The solid and dashed lines are the best linear fits using σ_c (as in Fig. 1*b*) and v_{rms}, respectively.

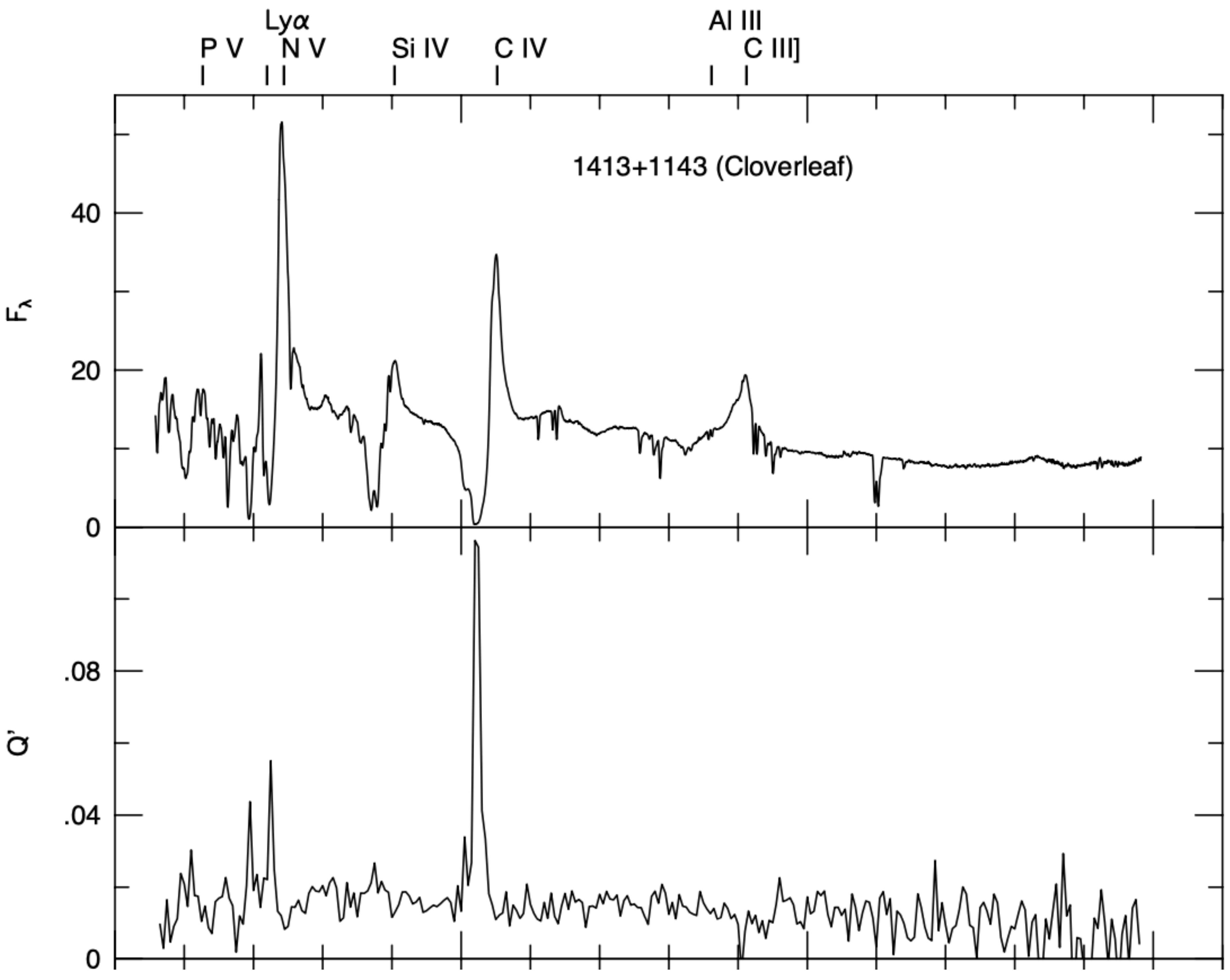

Ogle+ 1999

BAL Outflows

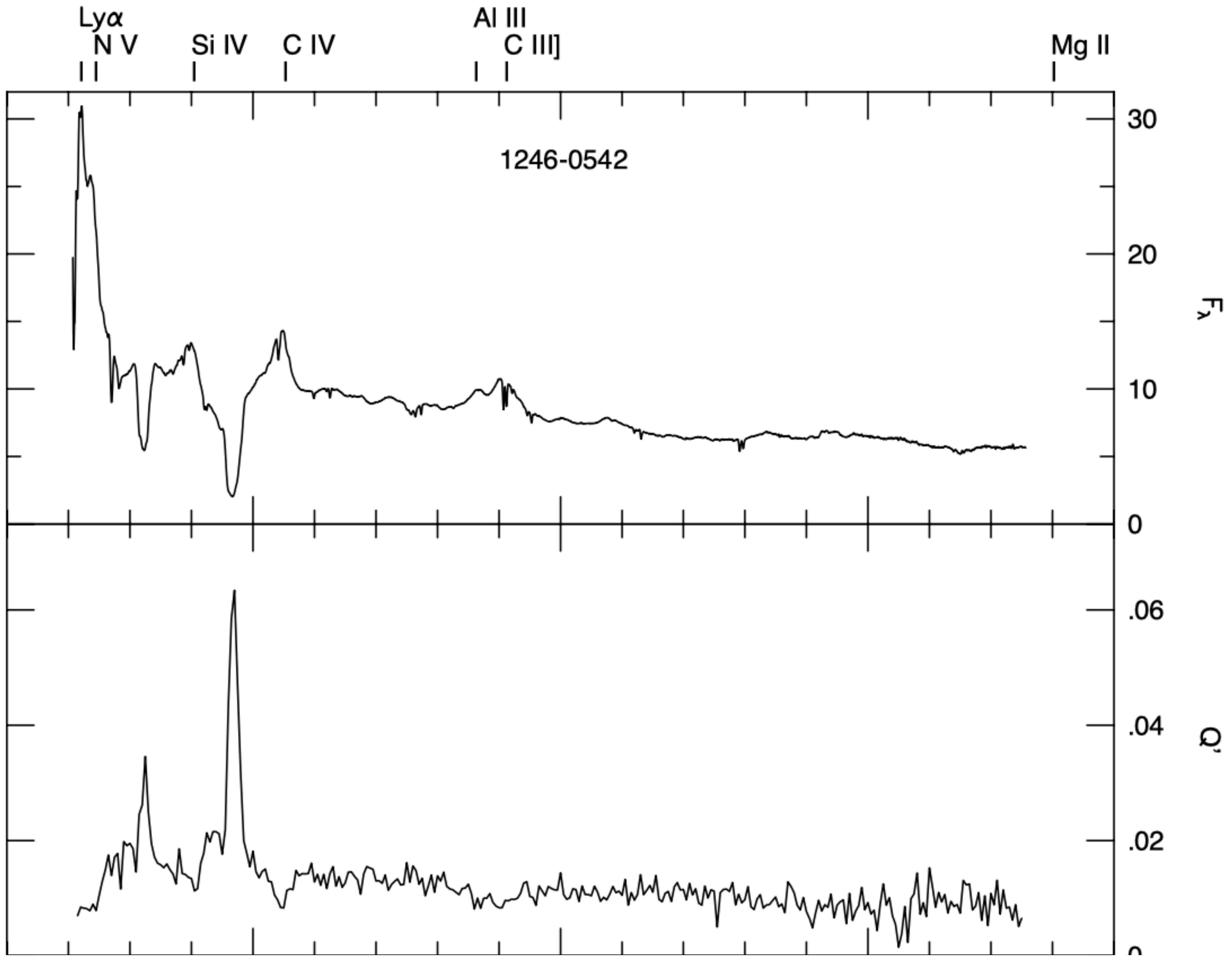

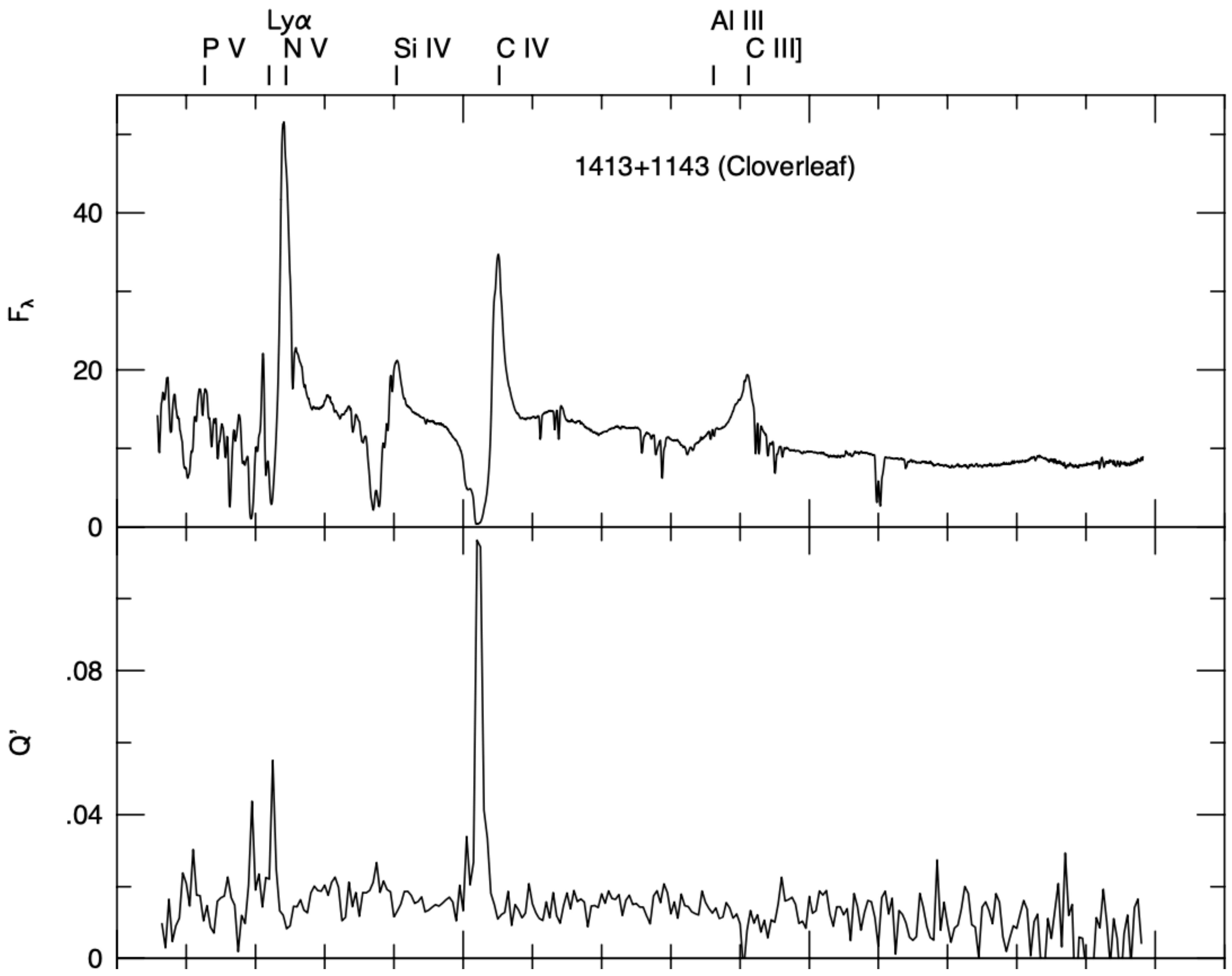

BAL Outflows

- Wind luminosity = $1/2\ dM/dt\ v^2 = 1/2\ \Omega R^2 \rho v^2$
- Momentum loss rate = $dM/dt\ v = \Omega R^2 \rho v$
- Measure v directly
- Estimate ρ
- Need R

Asteroseismology

Internal differential rotation

- Solar dynamo is driven by differential rotation
- Stellar magnetic fields produce x-rays and the bulk of the UV flux
- X-rays and UV evaporate protostellar disks
- X-rays and UV can strip planetary atmospheres

<u>Larson & Schou (2018)</u>

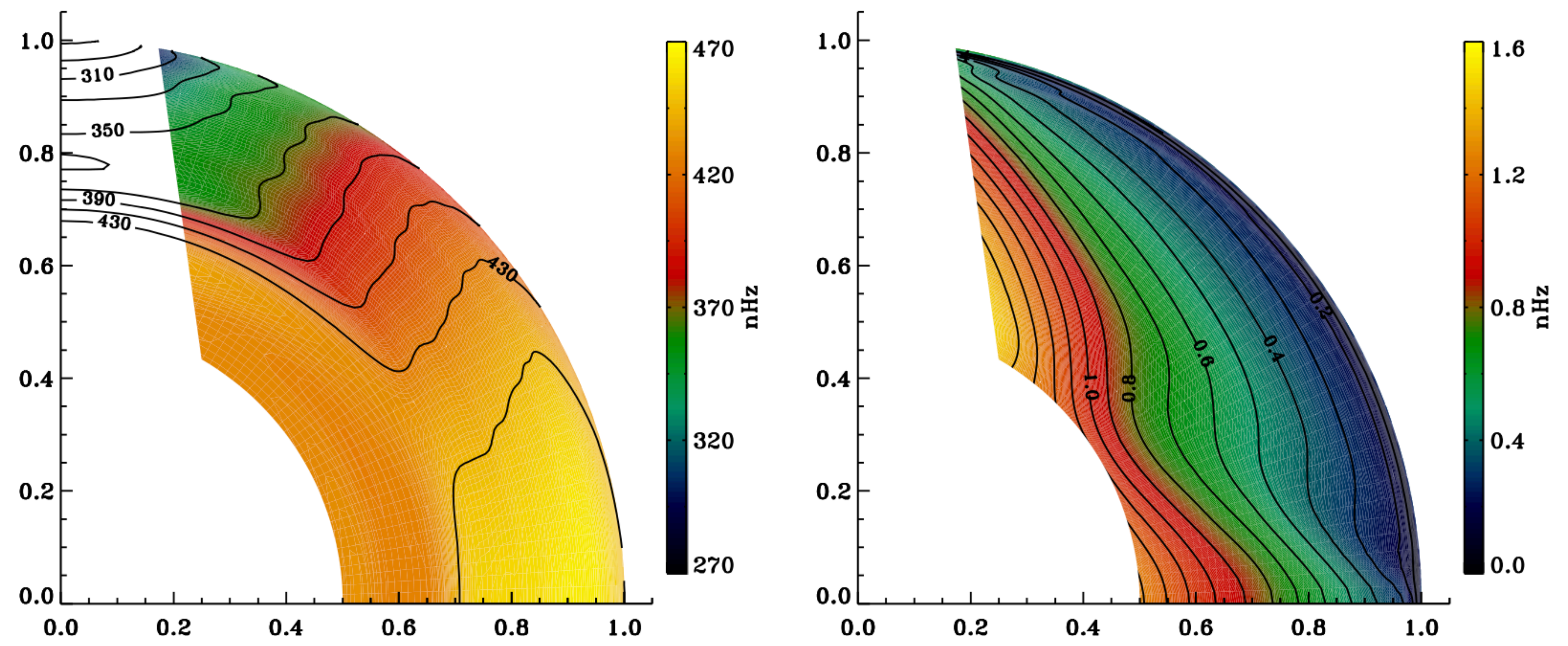

Figure 29 Internal rotation (*left*) and the corresponding errors (*right*) derived from the MDI full-disk analysis averaged over all Dynamics Runs. We have erased color from the regions where estimates of rotation are deemed unreliable; contours are retained on the left for ease of labeling.

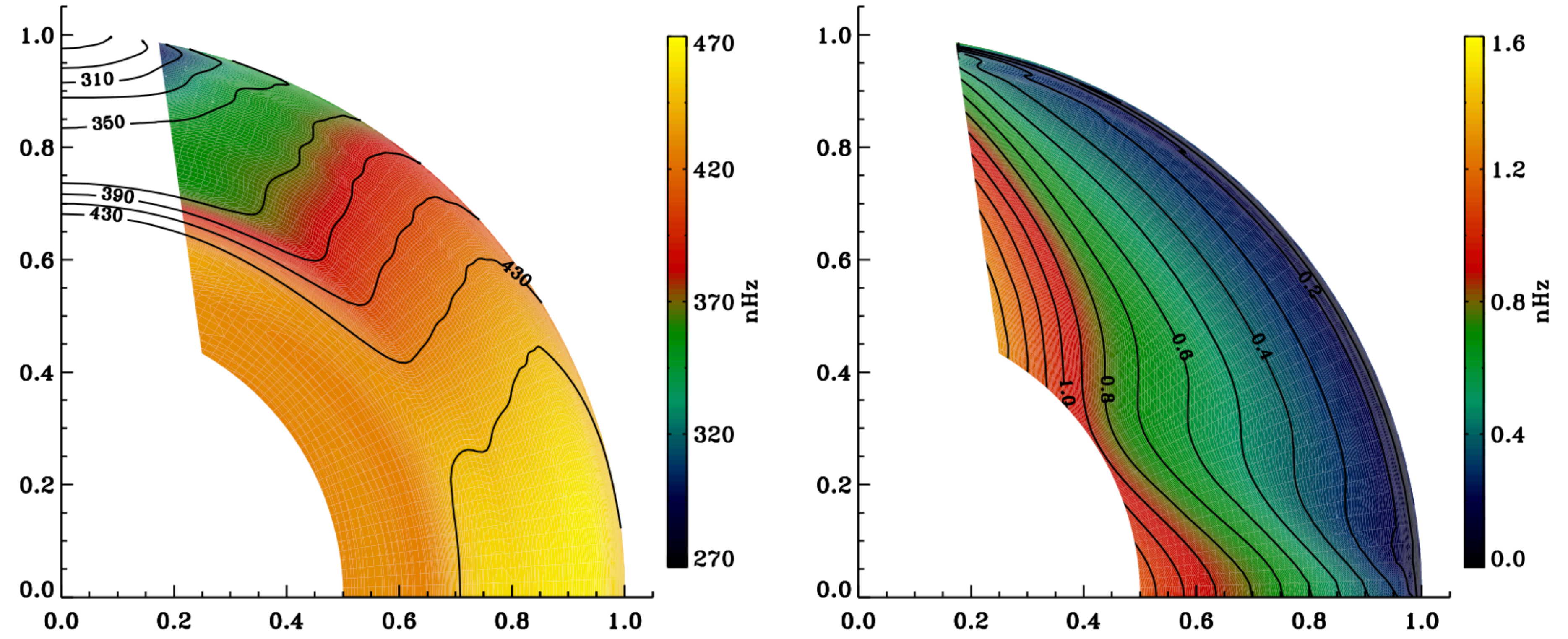

Figure 30 Internal rotation (*left*) and the corresponding errors (*right*) derived from an average over the first six years of the HMI 72-day analysis. We have erased color from the regions where estimates of rotation are deemed unreliable; contours are retained on the left for ease of labeling.

Helioseismology

Internal differential rotation

230 M. LAZREK ET AL.

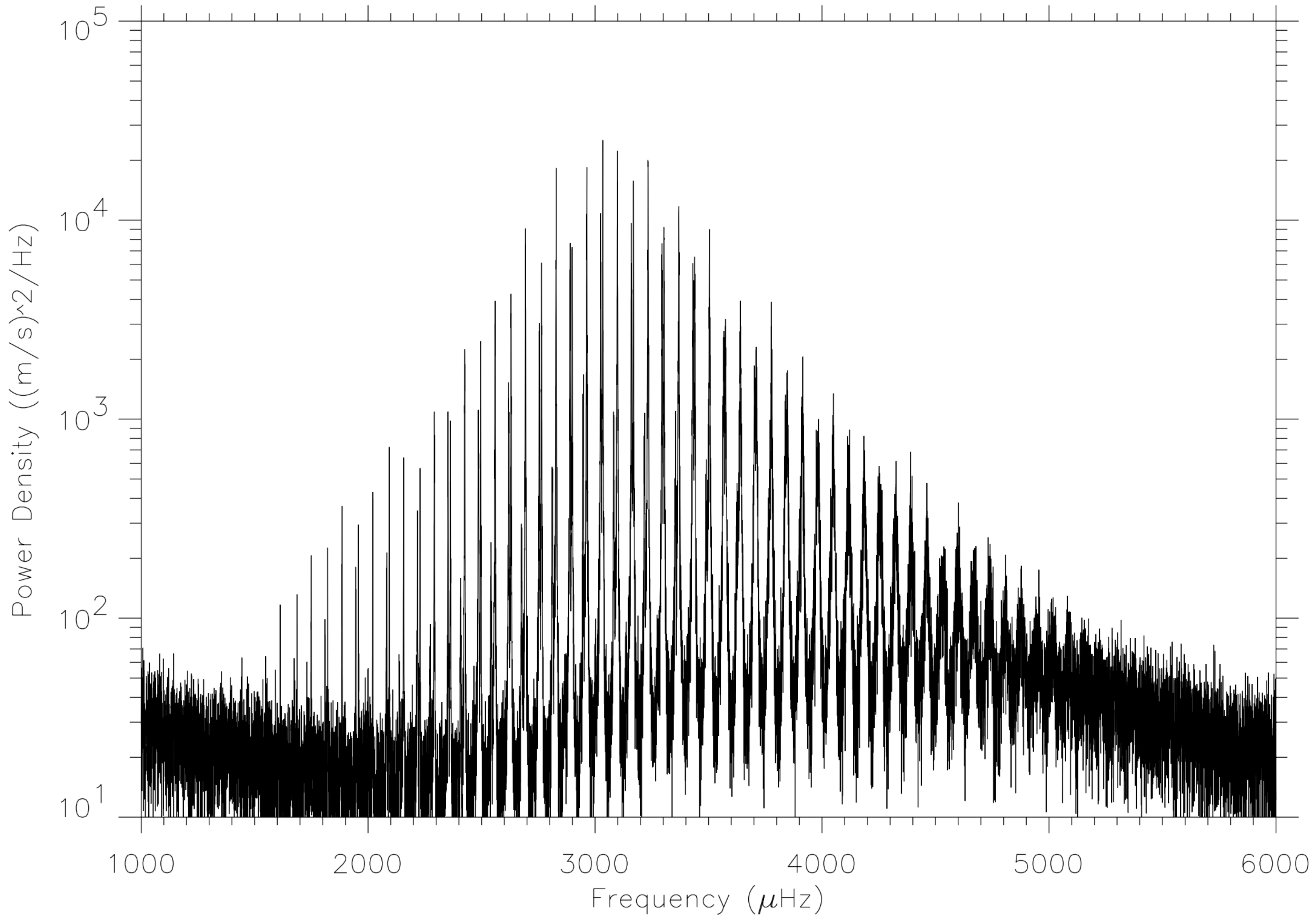

Figure 1. The acoustic *p*-mode spectrum of the Sun, as measured using the first eight months of GOLF data. At 3 mHz the ratio S/N is ∼3000.

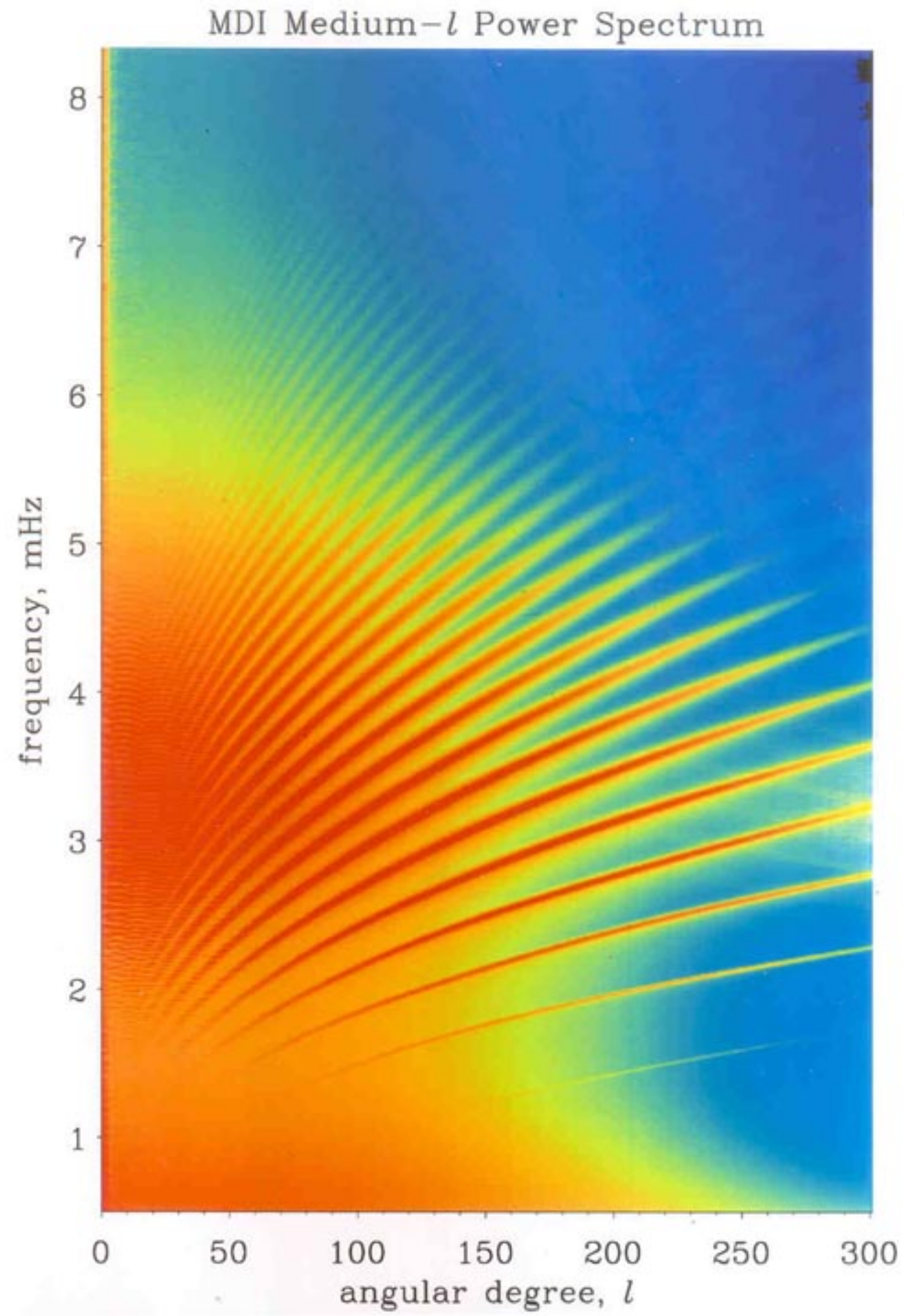

- Resolved stellar oscillation velocity power spectra

Helioseismology

Internal differential rotation

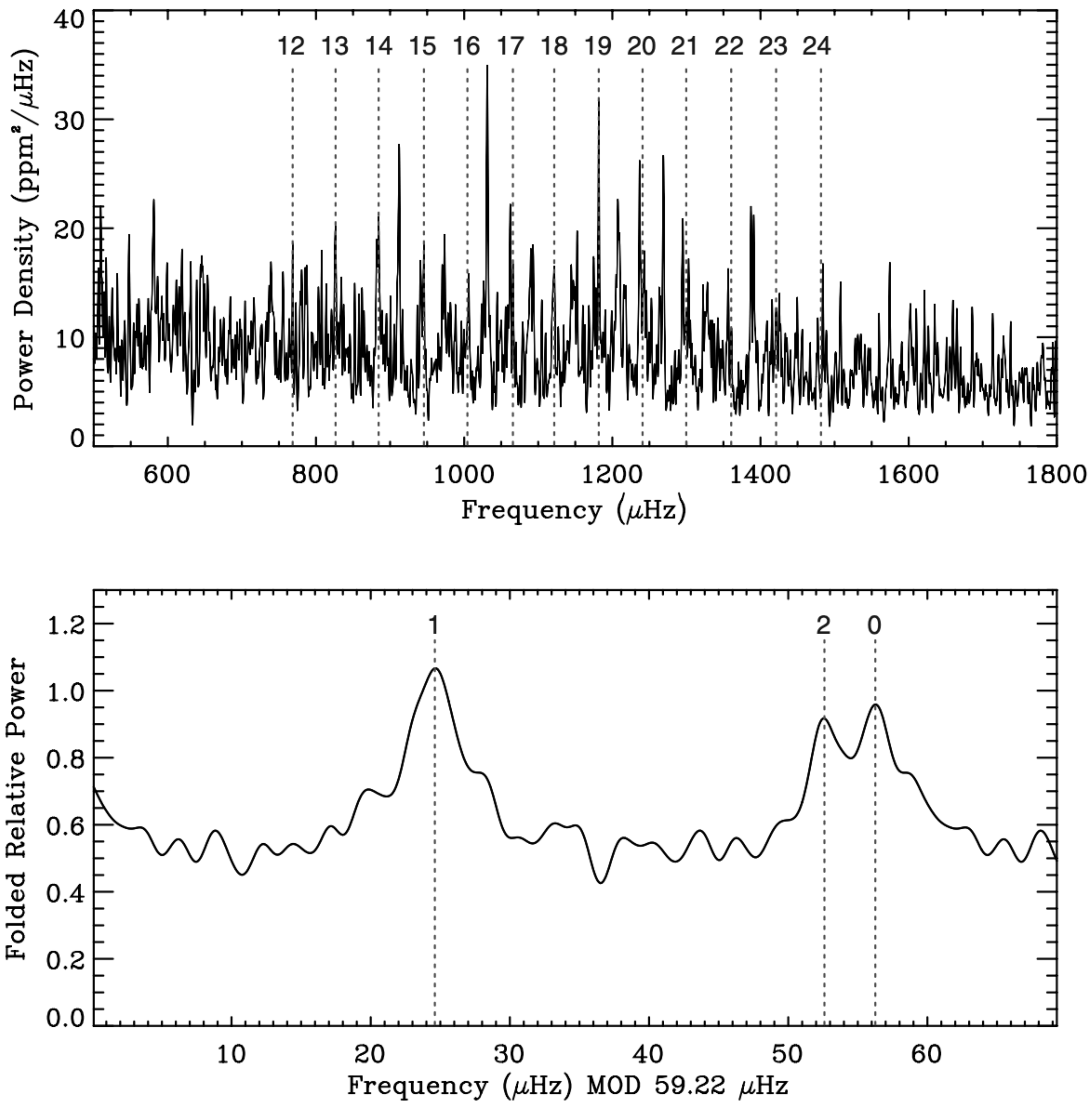

Helioseismology

Internal differential rotation

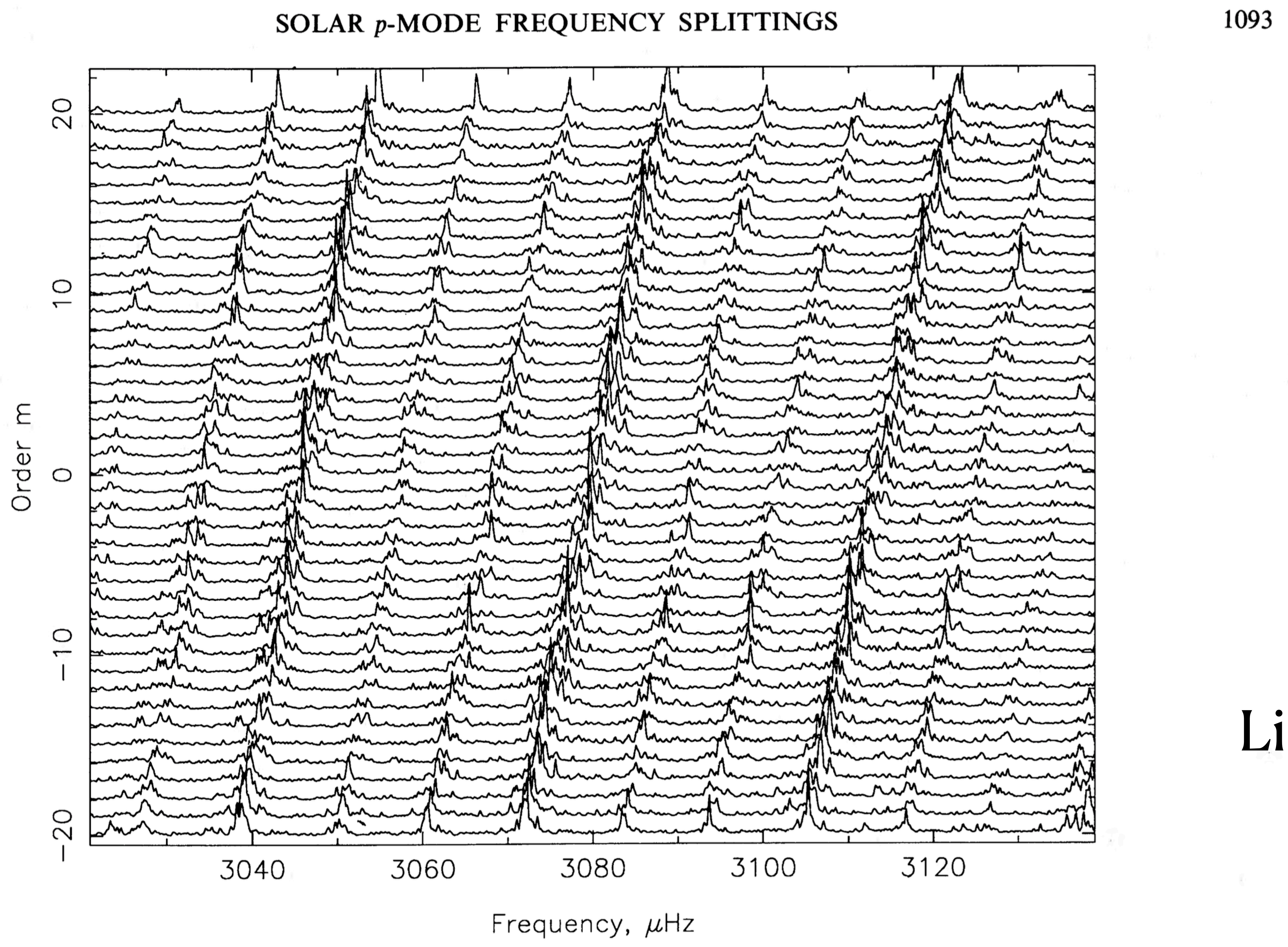

Libbrecht 1989

Helioseismology

Internal differential rotation

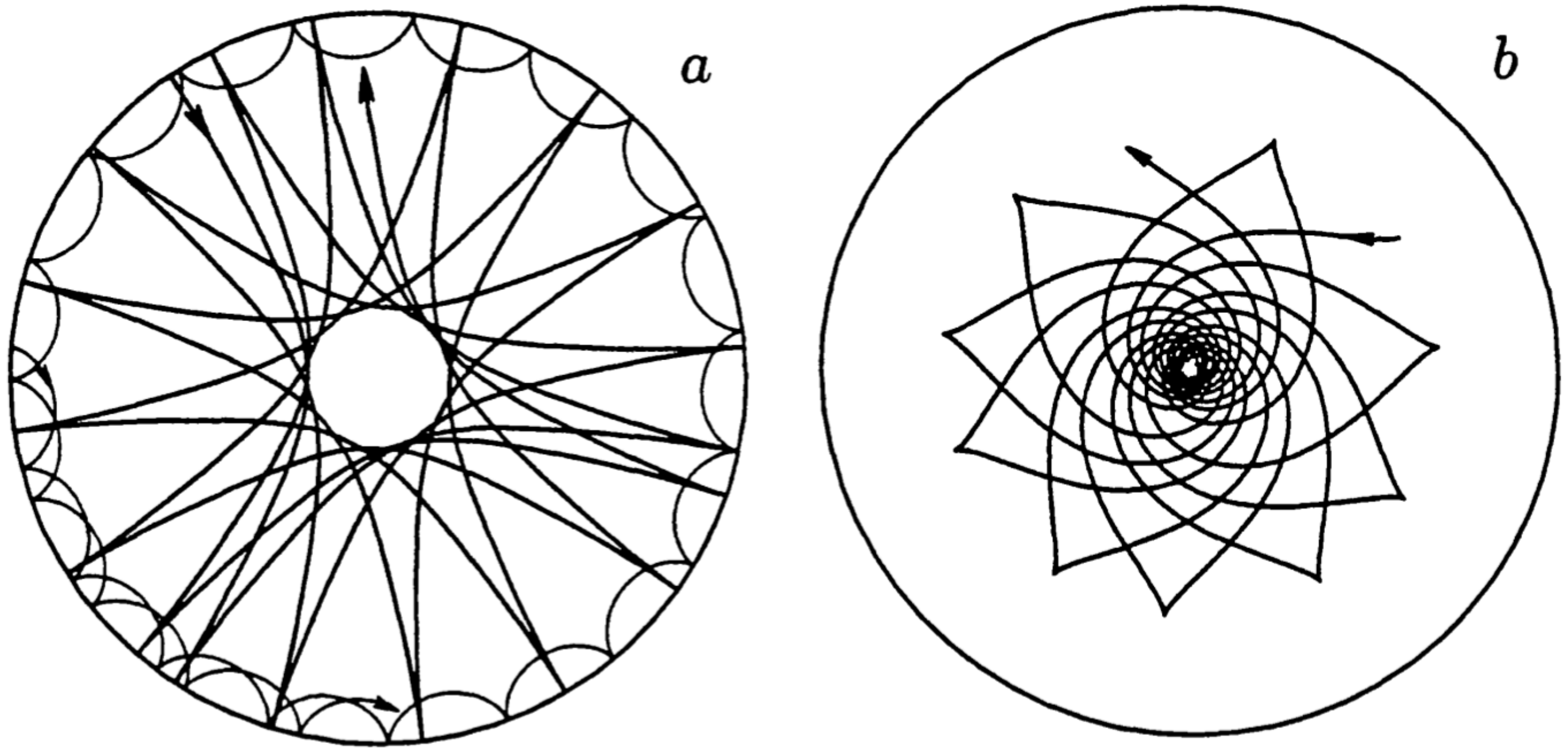

Figure 2 Ray paths in the standard model of the sun represented by the continuous line in Figure 1: (*a*) for two acoustic waves; the more deeply penetrating wave is p_8 ($l = 2$) and the shallower wave is p_8 ($l = 100$); (*b*) for the gravity wave g_{10} ($l = 5$). Note that the number of reflections per revolution is not integral, and indeed is almost never rational, so the ray paths

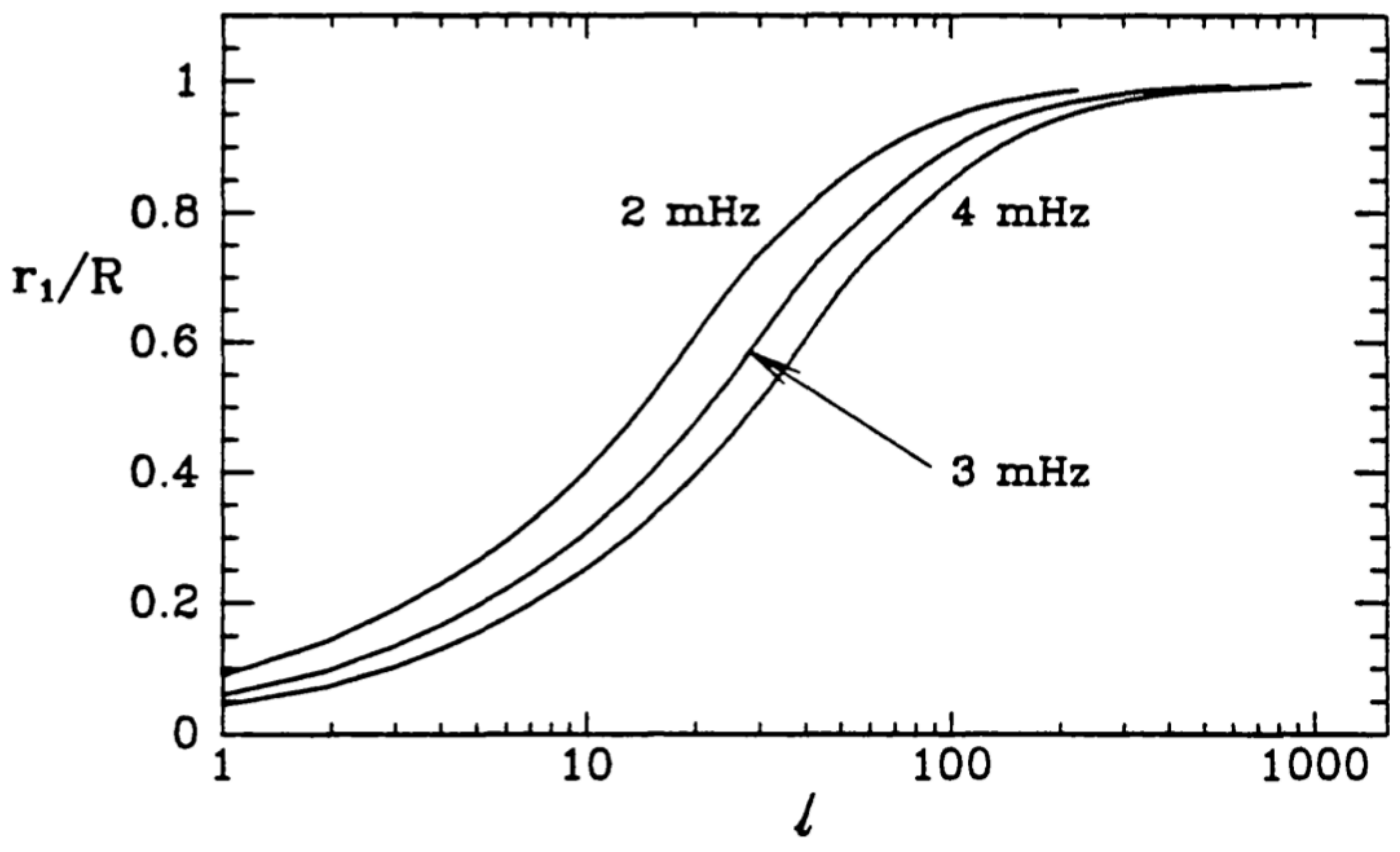

Figure 3 Lower turning points for *p* modes of a solar model, determined by the vanishing of κ, plotted against degree l for the three cyclic frequencies $\nu = \omega/2\pi = 2, 3, 4$ mHz. The curves for 2 and 3 mHz terminate at the lowest-order modes, at values of l determined by Equation 3.2 with $n = 1$.

Helioseismology

Sound speed v. R

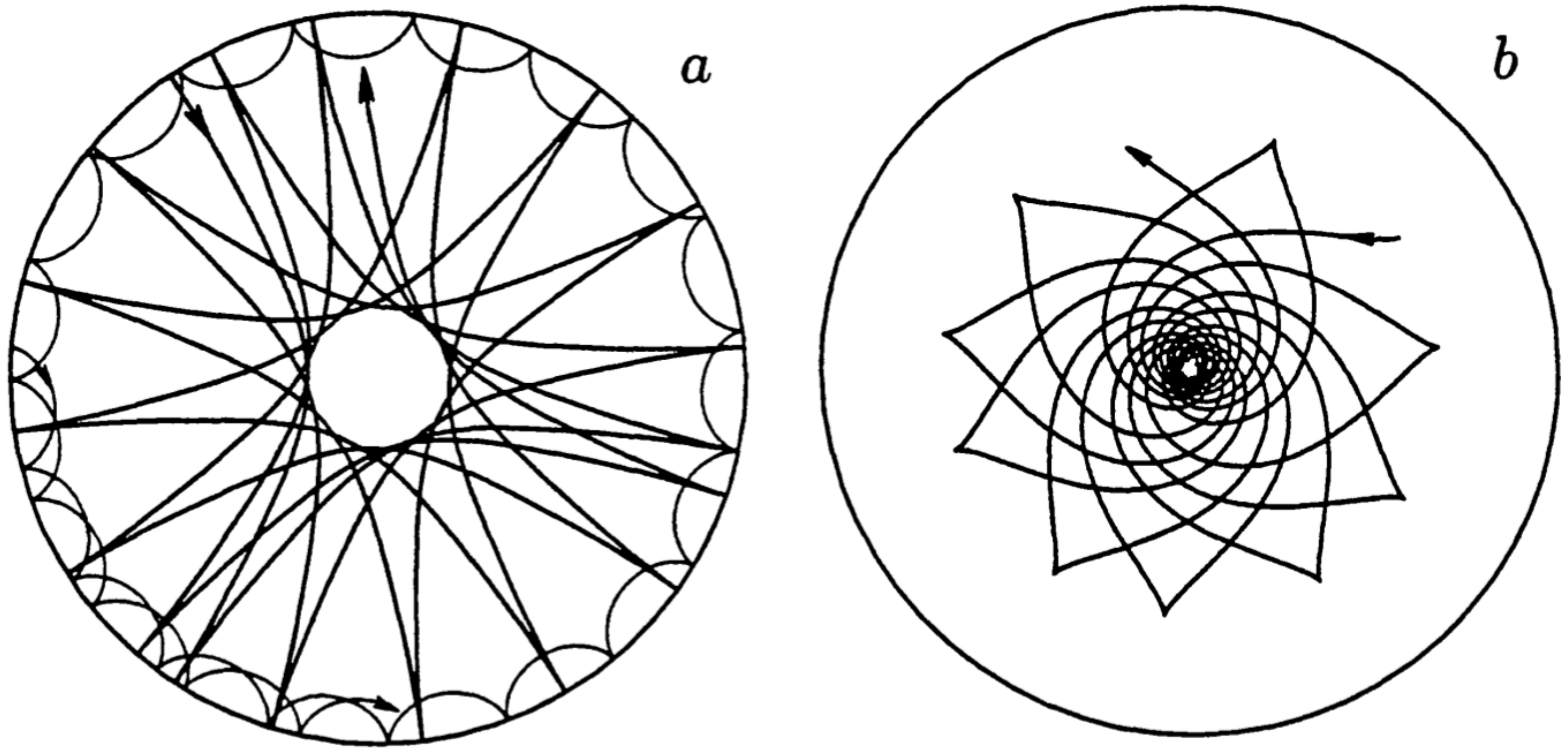

Figure 2 Ray paths in the standard model of the sun represented by the continuous line in Figure 1: (*a*) for two acoustic waves; the more deeply penetrating wave is p_8 ($l = 2$) and the shallower wave is p_8 ($l = 100$); (*b*) for the gravity wave g_{10} ($l = 5$). Note that the number of reflections per revolution is not integral, and indeed is almost never rational, so the ray paths

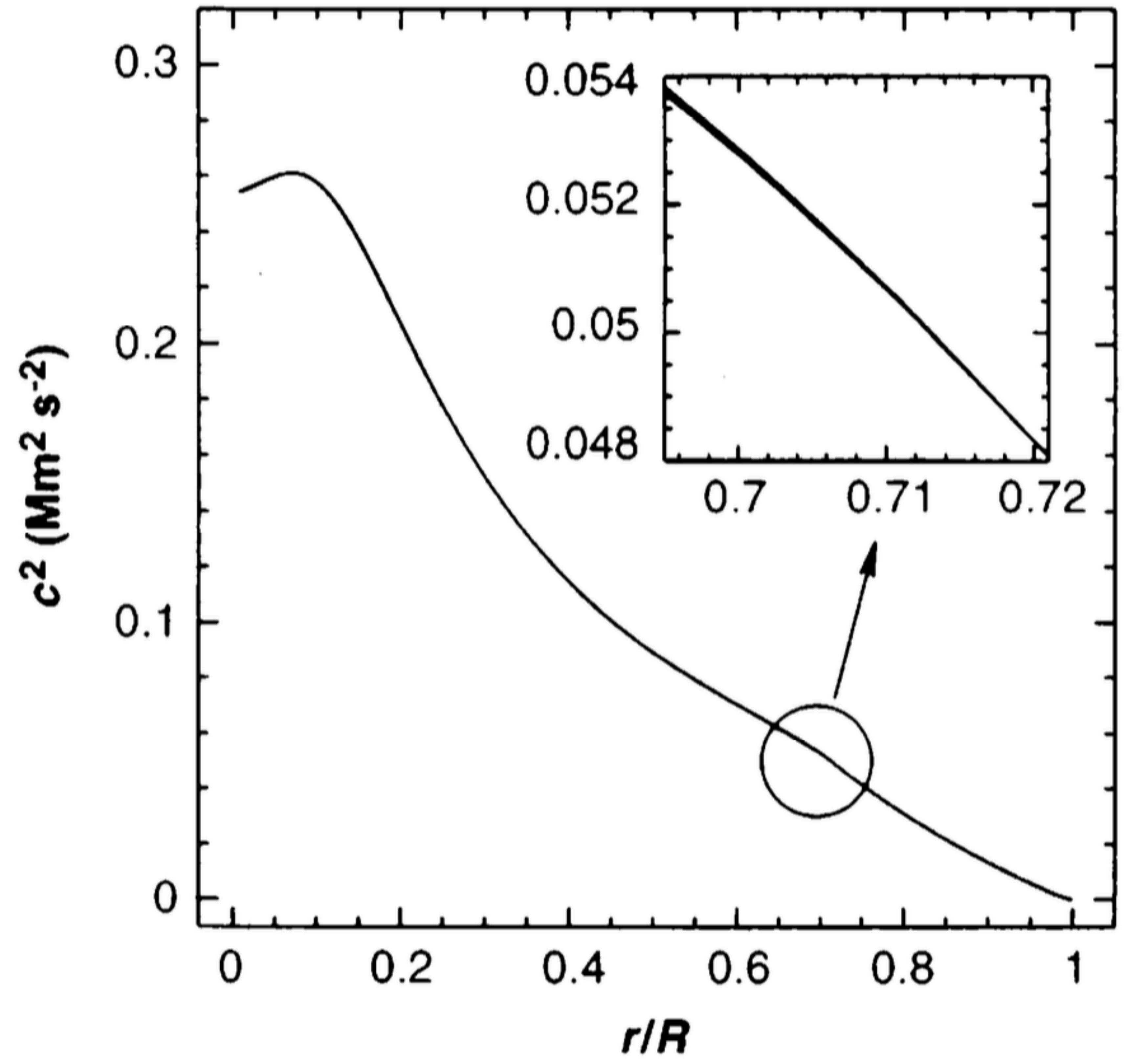

Fig. 3. The dashed curve is the square of the spherically averaged sound speed in the sun. The solid curve corresponds to a standard theoretical model. The magnitudes of the slopes of the curves are lower immediately beneath the convection zone, where the temperature gradient is too small to drive the instability. The inset shows that the convectively unstable region of relatively high slope extends somewhat more deeply into the sun than it does in the model.